To the Graduate Council:

I am submitting herewith a thesis written by Rebecca Ann Bachschmidt entitled "The Effect of Geometric Parameters on the Flow of Compressed Air Through Small Orifices." I have examined the final copy of this thesis for form and content and recommend that it be accepted in partial fulfillment of the requirements for the degree of Master of Science, with a major in Engineering Science.

Richard J. Jendrucko

Richard J. Jendrucko, Ph.D., Major Professor

We have read this thesis
and recommend its acceptance:

Jack Wasserman

Osama Soliman

Accepted for the Council:

C W Minkel

Associate Vice Chancellor
and Dean of the Graduate School

STATEMENT OF PERMISSION TO USE

In presenting this thesis in partial fulfillment of the requirements for a Master's degree at The University of Tennessee, Knoxville, I agree that the Library shall make it available to borrowers under rules of the Library. Brief quotations from this thesis are allowable without special permission, provided that accurate acknowledgement of the source is made.

Permission for extensive quotation from or reproduction of this thesis may be granted by my major professor, or in his absence, by the Head of Interlibrary Services when, in the opinion of either, the proposed use of the material is for scholarly purposes. Any copying or use of the material in this thesis for financial gain shall not be allowed without my written permission.

Signature Rebecca Bachschmidt

Date July 23, 1992

THE EFFECT OF GEOMETRIC PARAMETERS ON THE FLOW OF COMPRESSED AIR THROUGH SMALL ORIFICES

A Thesis Presented for the
Master of Science Degree

The University of Tennessee, Knoxville

Rebecca Ann Bachschmidt
August 1992

ACKNOWLEDGEMENTS

I would like to thank my major professor, Dr. Richard Jendrucko, for his guidance, patience, and commitment to excellence. I would also like to thank the other committee members, Dr. Osama Soliman for his invaluable assistance and Dr. Jack Wasserman for his advice and use of laboratory facilities. I would also like to thank Mr. Jack Brown for his assistance in constructing the experimental testing apparatus. Finally, I would like to thank the United Cities Energy Products Company for their technical assistance and loan of flow metering equipment.

ABSTRACT

An investigation was undertaken to determine the effect of cross-sectional geometry on the discharge of compressed air through thin orifices and to establish its relevance in the prediction of air lost in typical leakages found in industrial compressed air systems. Tests were conducted with four custom-fabricated circular and equilateral triangular orifices ranging size from $1.39(10)^{-3}$ to $0.21(10)^{-3}$ in^2 and $1.04(10)^{-3}$ to $0.18(10)^{-3}$ in^2, respectively, with thicknesses approximately 75% of the orifice hydraulic diameter. A compressed air orifice flow metering system was constructed to provide a constant-pressure source of dry, clean air at 100 psig and to meter the volumetric flow of air discharged through the orifices to the atmosphere. Flow approach velocity at the orifice upstream face was negligible; Reynolds numbers based on orifice diameter and maximum adiabatic compressible fluid velocity exceeded 100,000 for all experimental runs.

Coefficients of discharge calculated for the air mass flow rate through the circular orifices were about 5% higher than previously documented results for knife-edged circular orifices. However, throat thicknesses of the orifices used in investigation were about 10% greater, indicating a higher range of discharge coefficient possibly due to a decreased degree of efflux vena contracta.

Generally, the results indicated mass flow rates which were about 30% higher through equilateral triangular orifices than through circular orifices of the same cross-sectional area. Comparison of mass

flow rates obtained with triangular and circular orifices of equal hydraulic diameter again revealed discharge rates through the triangular orifices which were about 30% greater than those through the circular orifices. Although the hydraulic diameter concept closely approximates flows for a variety of duct geometries, it does not appropriately describe flows through thin orifices. Similar discharge flow rates were noted for triangular and circular orifices of equal perimeter. While the larger perimeter ratio of triangle to circle may in part explain an increased mass flow rate, the influence of orifice perimeter on the downstream flow pattern is believed to be significant. Therefore, it is concluded that orifice cross-sectional geometry is of primary importance in determining flow discharge rates.

Table of Contents

List of Tables

List of Figures

List of Symbols

A	minimum cross-sectional area
c	speed of sound
c_p, c_v	specific heats
C_d	discharge coefficient
d	diameter of orifice
D	diameter of approach
D_h	hydraulic diameter $D_h=4A/p$
E	energy
g_c	gravitational constant
h	enthalpy
k	specific heat ratio $k=c_p/c_v$
l	orifice length
L	distance along approach pipe center-line
$\dot{m}$	mass flow rate
M	Mach number
p	perimeter
P	upstream pressure
ΔP	differential pressure across orifice
q	heat per unit mass
Q	volumetric flow rate
R	gas constant
Re_{D_h}	Reynolds number based on orifice hydraulic diameter $Re_d=\rho V D_h/\mu$

Re_D	Reynolds number based on approach pipe diameter $Re_D=\rho VD/\mu$
T	upstream temperature
u	internal energy
V	velocity
w	work per unit mass
W	work
x,y,z	Cartesian coordinates

Greek Symbols

β	diameter ratio (d/D)
Y	expansion correction factor
K	flow coefficient
μ	dynamic fluid viscosity
ρ	fluid density

Subscripts

c	circumscribed circular area
i	inscribed circular area
m	mean
o	stagnant condition
t	triangular area
1,2	measurement stations

CHAPTER 1

INTRODUCTION

Compressed air is one of the most important and frequently used manufacturing energy forms. By increasing the pressure and energy content per cubic foot of air, compressed air systems provide a storable and easily distributable energy source to meet a plant's variable power demand requirement. United States industries' estimated electrical energy use to compress air exceeds one-half quadrillion BTU annually (1984) (1) and continues to grow as does industry itself. Therefore, compressed air is a substantially important commodity which should be used efficiently in order to save both energy and money in manufacturing facilities.

The following are common causes of energy losses in air distribution systems: 1) leaks, 2) line restrictions causing pressure drops, 3) production of a higher-than-needed system pressure, 4) indiscriminate air use, and 5) irregular replacement or adjustment of components such as filters, regulators, and mechanical drives. Among all of these, escaping air due to leaks results in the most lost compressed air energy; as much as 10% to 40% of overall compressed air capacity may be lost due to leaks in a typical plant (2).

Leaks may occur at any intrapipe connection, for example around worn fittings, in defective gaskets, at relief valves, and in couplings on tools, or in distribution lines. In most instances these leakages are due to poor piping maintenance rather than to incorrect equipment installation. More than in most other industrial systems, maintenance has a significant effect on compressed air systems; inadequacies result in decreased operational efficiency and in increased energy consumption. However, air leaks are often overlooked or are tolerated as the escaping air is nontoxic, odorless, and invisible. Frequency of leakage occurrence is high; 122 recommendations to repair one or more compressed air system leaks in 227 plants were made by the University of Tennessee's Energy Analysis and Diagnostic Center over a recent several-year period (3).

In order to justify maintenance repairs, it is desirable to quantify the energy costs associated with system leaks. While individual leaks may be minor, the cumulative effect of many leaks results in a significant continuous and unnecessary loss of increasingly costly energy. As electricity costs represent the major component in expenses associated with operating an air compressor, expenditures for repairs are usually rapidly recoverable in energy savings.

A typical method for estimating total system leakage rate is to fully pressurize the system, unload the compressor, and note the pressure decay time. An estimation of the percentage of compressor capacity used to supply air leakage may be made by operating a compressor with no process air in use and comparing the time that the compressor operates under load to the time of one complete load-unload cycle. Both of these system-level approaches provide an adequate, order-of-magnitude estimate of total system leakage but require comparison to a pre-determined compressor baseline operational pattern.

Another widely-used procedure for determining air loss is to identify individual leak sites and to estimate the leakage rate through each with the aid of mass flow rate prediction tables which are based on simple one-dimensional, choked flow theory and experimental correlations for idealized, circular orifice geometries. Difficulties with such procedures are two-fold. Firstly, for an accurate assessment of total air lost, a meticulous, time-consuming inspection of distribution lines must be made with either soapy water or acoustic detectors in an attempt to locate all leaks. Secondly, as typical mass flow rate prediction tables are generated for orifices of simple circular cross-section, an estimation of "equivalent circular leak area" must be made for comparison with tables. Leak geometries, however, are rarely circular in cross-section; most are quite irregular, such as slits in hoses or around loosened threads on fittings.

In view of the limitations of available data and methods for leak quantification and in order to focus on geometric factors which quantitatively determine air flow rates through actual leaks, more research is needed. In this way the actual energy cost of leaks with realistic geometries could be used to demonstrate the need for an improved maintenance program of leak repair, possibly for certain types of leaks in particular.

CHAPTER 2

BACKGROUND

THEORETICAL CONSIDERATIONS

To provide a better understanding of the presently utilized analytical expressions for predicting orifice mass flow rates and to establish the framework for a model describing realistic leak geometries, a brief review of the theoretical dynamic and thermodynamic foundations of compressible flow is in order. A compressible flow is described as one which exhibits significant density changes in at least one region of the flowing medium. These variations result principally from substantial pressure and temperature changes in the flow field. Governing equations include the conservation of fluid mass, momentum, and energy, and the perfect gas equation of state which is a material-specific constitutive relationship. While some limited, idealized compressible flow situations have been usefully analyzed from this governing equation set either by direct mathematical solution or with the aid of numerical techniques, for many realistic flow situations an analysis is simplified substantially with the assumptions of steady, one-dimensional flow.

Equations describing orifice flow are derived from the first law of thermodynamics which in its most general differential form for a closed system is:

$$dE = dQ - dW \qquad (2\text{-}1)$$

where E includes internal (u), kinetic, and potential energy forms, Q denotes heat added, and W represents work done by a system. For steady, assumed one-dimensional flow, with one inlet and outlet, an integrated form of Equation (2-1) may be written as:

$$\dot{q} - \dot{w} = -\dot{m}_1 (h + 1/2V^2 + gz)|_1 + \dot{m}_2 (h + 1/2V^2 + gz)|_2 \qquad (2\text{-}2)$$

where enthalpy, h, is defined in terms of internal energy,

$$h = u + P/\rho \qquad (2\text{-}3)$$

and w includes other than pressure-volume work. As can be readily derived with use of the continuity equation,

$$\dot{m}_1 = \dot{m}_2 \qquad (2\text{-}4)$$

the one-dimensional energy equation may be expressed as:

$$(h + 1/2\ V^2 + gz)|_1 = (h + 1/2\ V^2 + gz)|_2 - q + w \qquad (2\text{-}5)$$

Application of an adiabatic assumption outside of the thermal and velocity boundary layers where heat transfer and viscous effects are by definition zero reduces the form of the one-dimensional energy equation to:

$$(h + 1/2\, V^2)|_1 = (h + 1/2\, V^2)|_2 = constant = h_o \qquad (2\text{-}6)$$

Potential energy changes have been neglected as their magnitude is extremely small in comparison to kinetic energy and enthalpy changes in typical flows. The stagnation enthalpy of the flow, h_o, is the maximum enthalpy which the fluid would attain if brought to rest adiabatically.

Assumption of a perfect gas,

$$P = \rho RT \qquad (2\text{-}7)$$

where R is the gas constant given by the difference in a particular gas' specific heats

$$R = c_p - c_v \qquad (2\text{-}8)$$

and

$$c_p = \frac{k}{(k-1)} R \qquad (2\text{-}9)$$

$$k = c_p/c_v \qquad (2\text{-}10)$$

permits expression of enthalpy as:

$$h = c_pT \tag{2-11}$$

Equation (2-6) reduces to:

$$(c_pT + 1/2\ V^2) = c_pT_o \tag{2-12}$$

Maximum fluid velocity is obtained when enthalpy and temperature are considered to drop to absolute zero:

$$V_{max} = (2h_o)^{1/2} = (2c_pT_o)^{1/2} \tag{2-13}$$

For most compressible gas flow analyses the frequent assumption of a perfect gas acceptably models properties of real gases. The variable on which specific heat depends most significantly is temperature. However, for typically encountered temperature ranges the effects on specific heat are relatively minor. For air the value of specific heat increases only about 30% as temperature increases from 0 °F to 5000 °F (4). Therefore, assumption of the perfect gas law is reasonable in the study of orifice air flows at ambient temperature.

Further restricting the analysis to an isentropic case, the critical flow state may be examined. Theoretical, thermodynamically ideal, isentropic flow is considered critical when fluid velocity equals the speed of sound (c) in that fluid; Mach number is defined as

$$M = V/c \tag{2-14}$$

and equals 1.0 for critical flow. This may occur only when the fluid passes through a minimum cross-sectional area. (Compressible flows in general are characterized by Mach numbers greater than 0.3.)

Physically, the speed of sound,

$$\{k(\partial P/\partial \rho)\big|_T\}^{1/2} \qquad (2\text{-}15)$$

is the propagation rate of a pressure wave of infinitesimal strength through a still fluid and in effect defines a maximum compressible fluid flow velocity in response to a local pressure gradient. Temperature gradients, which are indeed small, are considered to be only within the interior of the wave with no velocity gradients on either side. Nearly reversible and adiabatic, propagation of pressure waves may be considered isentropic. Noting that for a perfect gas the relation between pressure and density in an isentropic process is $kP/\rho = constant$, the speed of sound for a perfect gas can be expressed as:

$$c = (kP/\rho)^{1/2} = (kRT)^{1/2} \qquad (2\text{-}16)$$

Maximum mass flow rate of a perfect gas at isentropic conditions may be derived with use of the definitions of Mach number and speed of sound in addition to simplified thermodynamic relationships. From the steady flow energy equation, Equation (2-12), and from the definition of specific heat, Equation (2-9), velocity may be expressed as:

$$V = \sqrt{2\ c_p\ (T_o - T)} = \sqrt{\frac{2\ k}{(k-1)} R\ (T_o - T)} \qquad (2\text{-}17)$$

Using the definitions of c_p and c, Equations (2-9) and (2-16) respectively, the stagnation temperature ratio takes the form:

$$\left(\frac{T_o}{T}\right) = 1 + \left(\frac{(k-1)}{2}\right)\left(\frac{V^2}{c^2}\right) = 1 + \left(\frac{(k-1)}{2}\right) M^2 \qquad (2\text{-}18)$$

Substituting the following relations between P, T, and ρ for an isentropic process of a perfect gas,

$$\left(\frac{P}{P_o}\right) = \left(\frac{\rho}{\rho_o}\right)^k \qquad (2\text{-}19)$$

$$\left(\frac{T}{T_o}\right) = \left(\frac{P}{P_o}\right)^{(k-1)/k} \qquad (2\text{-}20)$$

into Equation (2-18) yields pressure ratio as a function of Mach number:

$$\left(\frac{P_o}{P}\right) = \left[1 + \left(\frac{k-1}{2}\right) M^2\right]^{k/(k-1)} \qquad (2\text{-}21)$$

Substitution of the perfect gas equation, Equation (2-7), and the stagnation temperature ratio, Equation (2-18), into the continuity equation, Equation (2-4) (where $\dot{m} = \rho A V$), yields

$$\dot{m} = AM \sqrt{\frac{k\,g_c}{R}}\ \frac{P}{\sqrt{T_o}} \sqrt{1 + \frac{k-1}{2} M^2} \qquad (2\text{-}22)$$

Elimination of P from Equations (2-21) and (2-22) yields:

$$\dot{m} = A \sqrt{\frac{k\,g_c}{R}}\ \frac{P_o}{\sqrt{T_o}}\ \frac{M}{\left(1 + \frac{(k-1)}{2} M^2\right)^{(k+1)/2(k-1)}} \qquad (2\text{-}23)$$

For critical conditions, $M = 1$, the values $k = 1.4$ and $R = 53.3 \frac{ft\ lb_f}{lb_m\ ^o\mathrm{R}}$ for air, and the dimensional constant $g_c = 32.17 \frac{ft\ lb_m}{lb_f\ s^2}$ the theoretical maximum mass flow rate for a one-dimensional, isentropic flow becomes:

$$\dot{m} = 0.532 \frac{AP_o}{\sqrt{T_o}} \qquad (2\text{-}24)$$

This relationship is often referred to as Fliegner's formula (5) and is widely used to quantify compressed air flow through leaks.

APPROACHES TO QUANTIFICATION OF ORIFICE FLOW

Flow through an orifice, however, does not follow ideal flow law as does flow through a converging-diverging nozzle. Unlike a nozzle, the exit jet cross-sectional area is free to expand and as a result, mass flow rate has been shown to vary at and below that corresponding to the critical pressure ratio (6). Furthermore, system irreversibilities and energy losses due in part to viscous, thermal, compressibility, and three-dimensional effects prevent flow through an orifice from reaching the theoretical maximum. Thus, the discharge coefficient C_d is included in Fliegner's formula, Equation (2-24), to account for "real" system energy losses:

$$\dot{m} = 0.532\, C_d \frac{A P_o}{\sqrt{T_o}} \qquad (2\text{-}25)$$

Mass flow rate tables based on Equation (2-25) are often used for the estimation of compressed air leakage; such tables are frequently included in industry literature (7) and engineering handbooks (8,9). Tabulated are flow rates which correspond to various upstream pressures and circular orifice diameters. Commonly used values of C_d for gaseous flows are 0.97 for well-rounded and 0.61 for sharp-edged circular orifice entrances. Values reported for the discharge coefficient were determined experimentally utilizing orifice metering techniques (7). However, no experimental determination of discharge coefficients for orifice geometries other than circular is currently available in literature.

The purpose of this research is therefore, to evaluate the sensitivity of the discharge coefficient to orifice cross-sectional geometry and to establish its impact upon quantification of compressed air leaks through non-idealized geometries.

EMPIRICAL EQUATIONS DESCRIBING ORIFICE FLOW

Flow through circular orifices has been widely studied; in general, the motivation for study has been to improve commercial gas flow rate measurement techniques. Compressed air discharge through a circular orifice is schematically illustrated in Figure 1.

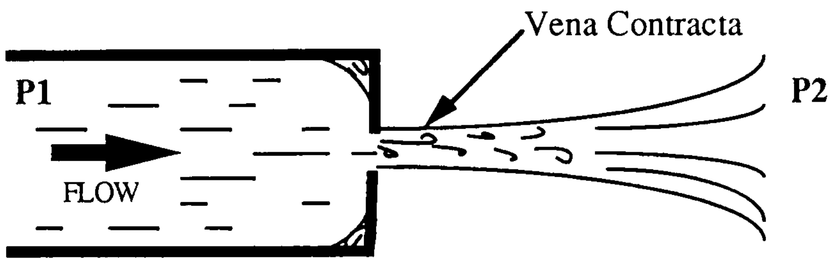

Figure 1. Schematic Representation of Fluid Flow Through an Orifice.

In 1916 H.B. Reynolds (10) described orifice flow with the following empirical equation, the general form of which is based on ideal compressible flow theory:

$$\dot{m} = 0.546 \frac{A}{\sqrt{T}} (P_1^2 - P_2^2)^{0.48} \qquad (2\text{-}26)$$

which is of a form similar to the Fliegner Equation, (2-24). While such improvements in predictive equations have been useful for certain flow situations, these relationships for all practical purposes are case-specific. Thus, Fliegner's Equation is still of primary utility in describing general orifice flow.

Subsequent work by Bean, Buckingham, and Murphy (11) used mean density, (ρ_m), defined as the density at the upstream temperature and at the average of upstream and downstream pressures, in the calculation of C_d:

$$\dot{m} = C_d \frac{0.525 d^2}{\sqrt{1 - \beta^4}} \sqrt{\rho m \ \Delta P} \qquad (2\text{-}27)$$

Indeed, stagnation properties, such as those for density, pressure, or temperature, do not exist as constants in "real" compressible orifice flow but in fact change with position in the flow direction due to flow irreversibilities. Interestingly, this approach resulted in coefficients of discharge for air flow that deviated only slightly from those obtained for water as determined by Bean, Buckingham, and Murphy (11).

In 1948 Perry (6) investigated the relationship between mass flow, pressure, temperature, and orifice area, deriving orifice flow equations in terms of an expansion correction factor, Y, and a flow coefficient K which combines the discharge coefficient C_d and the velocity approach factor $\sqrt{1 - \beta^4}$ to yield:

$$\dot{m} = AKY\sqrt{2g\rho\Delta P} \tag{2-28}$$

where

$$K = \frac{Cd}{\sqrt{1 - \beta^4}} \tag{2-29}$$

The derivation of Equation (2-28) is based upon the one-dimensional, conservation of energy and mass along with the use of empirical functions including equations of fluid state and thermodynamic process statements. Perry used this equation to describe the flow of compressible and incompressible homogeneous fluids through orifice meters. For either, the coefficient of discharge C_d was found to be approximately 0.6 and the flow coefficient K typically ranged from about 0.6 to more than 0.7.

Multiplicative correction factors such as K and Y are commonly used in the intended accurate but greatly simplified commercial orifice metering techniques for natural gas and other hydrocarbon fluids. Calibration sensitivity to additional parameters such as approach velocity profile and gas expansion can be represented with a composite orifice flow constant, C' , which for commonly metered fluids may be expressed as (12):

$$C' = F_b F_r Y F_{pb} F_{tb} F_{tf} F_{gr} F_{pv} \tag{2-30}$$

where: F_b = basic orifice factor (defined in terms of K)

F_r = Reynolds Number factor

F_{pb} = pressure base factor

F_{tb} = temperature base factor

F_{tf} = flowing temperature factor

F_{gr} = real gas relative density factor

F_{pv} = super-compressibility factor

However, some question exists concerning the mathematical independency of these factors (13).

For a given gas and flow geometry, the flow coefficient K and the expansion factor Y are empirical values which must be determined from test data. Bean, Buckingham, and Murphy (11) developed empirical equations to represent K for an orifice meter with either flange or pipe taps for several ranges of flow Reynolds number. Stolz (14) later proposed a simpler relationship suitable for any tapping arrangement:

$$K = 0.5959 + 0.0312\beta^{2.1} - 0.184\beta^{8} +$$
$$0.0029\beta^{2.5}\left(\frac{10^6}{Re_{D_1}}\right)^{0.75} + 0.09\left(\frac{L_1\beta^4}{1-\beta^4}\right) - 0.0337L_2\beta^3 \tag{2-31}$$

The discharge coefficient, C_d, often experimentally investigated, has also been mathematically derived from complex variable coordinate transformations of the streamline function for a circular orifice geometry. A jet escaping from a two-dimensional, sharp-edged, circular orifice was studied by Busemann (15) using the tangent-gas approximation, a mathematical technique which allows construction of compressible flows from incompressible ones. The theoretical results indicated a discharge coefficient of 0.61 for gaseous flows. For Mach numbers increasing to sonic, theoretical predictions qualitatively follow experimental results; both predict a rise in discharge coefficient due to compressibility effects. Such analytical techniques, however, would be impractical for the study of realistic, irregular leak geometries due to mathematical complexity.

DISCHARGE COEFFICIENT AS A FUNCTION OF FLOW PARAMETERS

The effects of several flow parameters on the discharge coefficient have been experimentally established. Perry showed fundamental differences between subcritical and critical orifice flow regimes (6). For pressure ratios below choked conditions, a plot of discharge coefficient versus pressure ratio is best described as elliptical. At and beyond critical conditions, C_d tends toward a constant value (Figure 2). The rate of mass flow through a converging nozzle increases until the discharge pressure becomes critical; further decreases in discharge pressure do not result in increased mass flow. In contrast, flow through a thin-plate orifice actually continues to increase in the critical region. Perry explained this phenomenon by noting that the exit jet cross-sectional area of the compressible fluid stream flowing through an orifice continues to expand as surrounding pressure decreases.

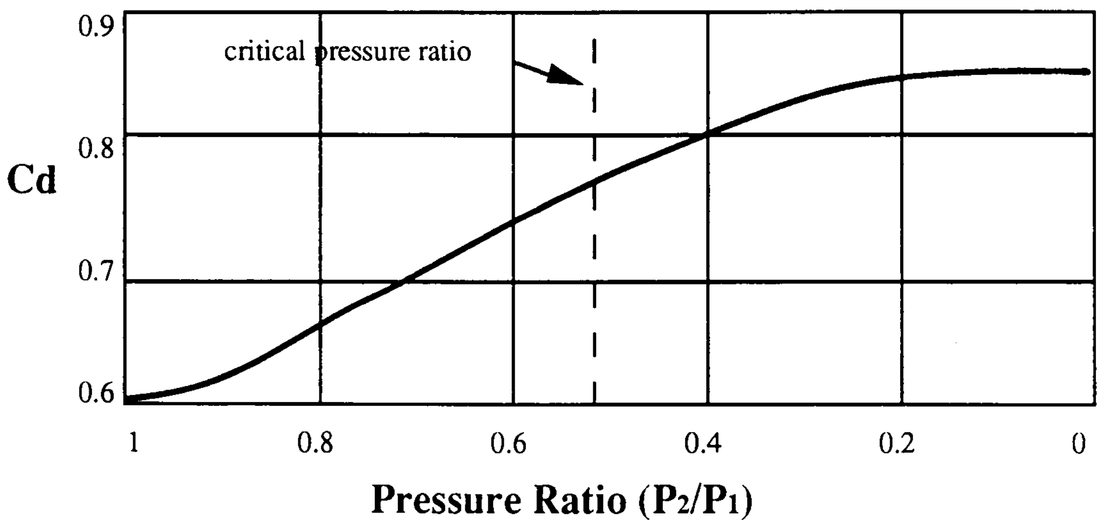

Figure 2. Discharge Coefficient vs Pressure Ratio for Flow Through Sharp-Edged Orifices with Zero Approach Velocity.
(Source: J.A. Perry, Critical Flow Through Sharp-Edged Orifices, *Trans. ASME*, vol. 71, 1949, p.762.)

The discharge coefficient as a function of Reynolds number has been investigated repeatedly with consistent trends identified (8). Generally, dependence of C_d on Reynolds numbers above 30,000 is minimal; correlation coefficients are found to be approximately constant in this range (Figure 3). In the transition region, $50 < Re < 30{,}000$, coefficient values are somewhat higher; in the laminar region, $Re < 50$, C_d is approximately proportional to the square root of Re. In 1989 Fox and Stark (16) similarly showed that the value of C_d also rises rapidly with Reynolds number for water flow to attain an approximately constant value termed the "ultimate discharge coefficient" in the region of Re=10^4 for miniature short-tube circular orifices. As Re increases, significant recirculation regions are established at the entrance to the flow passage and losses sustained in the vena contracta diminish considerably. This leads to an increase in C_d. With the onset of transitional flow at Re=2,000 and the establishment of fully turbulent conditions at Re > 4,000, the effects of viscosity are much reduced. Thus, further increases in Re in this region produce little change in the value of C_d and it tends toward a constant value.

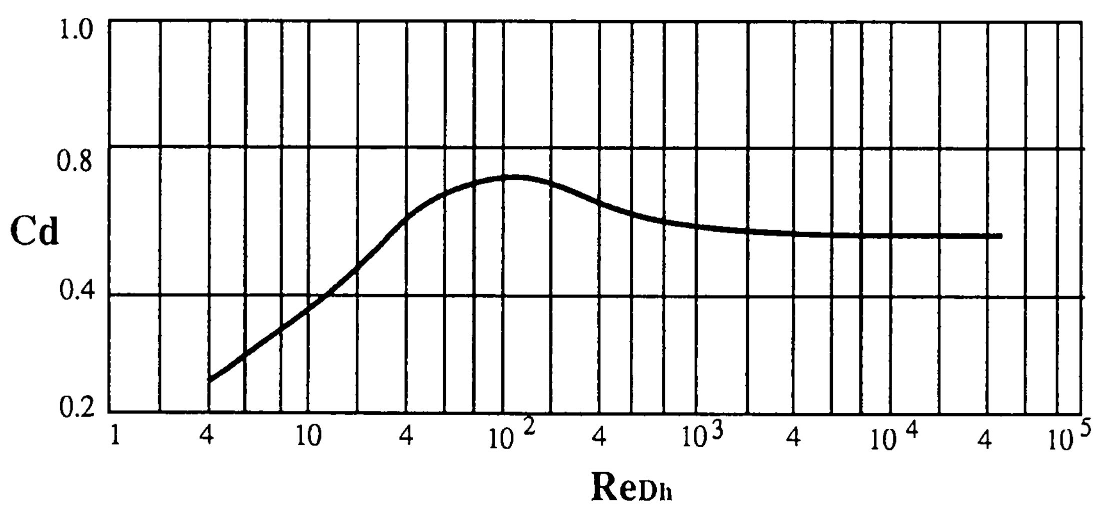

Figure 3. Discharge Coefficient vs Reynolds Number for the Discharge of Air Through Square-Edged Circular Orifices, β =0.20. (Adapted from: Tuve and Sprenkle, *Instruments*, vol. 6,1933, p.201.)

Many researchers have described the effect of small diameter orifices in terms of the orifice diameter to channel-of-approach diameter, the β ratio, which scales the influence of the approach flow velocity profile. In 1949 Linden and Othmer (17) found that in the viscous region the value of the discharge coefficient dropped with decreasing values of β. However, it approached an apparent minimum near $\beta = 0.2$ at which point a reversal trend was noted. Furthermore, they determined that β can be as high as 0.2 without affecting the assumption of negligible approach velocity. This implied that in the case of small β an effectively infinite fluid reservoir exists immediately upstream of the orifice inlet. For larger values of β there is an increased influence of the approach flow velocity.

The 1951 experiments of Grace and Lapple (18) documented the effect of orifice thickness on the discharge coefficient. For orifice plates one-hole-diameter thick used for $Re > 10^5$, the degree of vena contracta effectively decreases and thus, higher ranges of the discharge coefficient are obtained. However, at lower Re, frictional effects become more appreciable for thick plate orifices and flow reattachment possibly does not occur within the throat length. Thus, the discharge coefficients are reduced. Fox and Stark (16) also obtained similar results. For short-tube orifices between one- and fourteen-hole-diameters thick, a cavitation-induced flow separation from the boundary walls followed by only partial reattachment is observed. This instability, termed "hydraulic flip," occurs for specific pressure differentials which vary as a function of the orifice (l/d) ratio. Consequently, the associated discharge coefficient is reduced.

CHAPTER 3

EXPERIMENTAL DESIGN

OVERVIEW OF INVESTIGATION RATIONALE

The testing system was designed to meter the volumetric flow rates of compressed air through both idealized circular and non-circular orifices for comparison to predicted, theoretical volumetric flow rates and ultimately for the calculation of associated discharge coefficients. Orifices were specified to be thin, with thicknesses less than the overall orifice diameters, have flat, smooth upstream edges which were to be kept clean and free from the accumulation of dirt or other extraneous materials, to be centered within the orifice fittings, and to be installed perpendicular to the center-line axis of the upstream piping. The test equipment design was selected to provide a constant-pressure source of dry, clean air at a negligible velocity of approach through a minimum of straight, smooth-bore, clean pipe lengths. Finally, as industrial air-powered equipment is frequently designed for efficient operation with an input air pressure of 90 to 100 psig, the experimental system pressure was chosen as 100 psig with air to be discharged to the atmosphere in order to simulate an industrially realistic pressure drop.

MANUFACTURE AND SIZING OF TEST FLOW ORIFICES

Circular test orifices were designed and manufactured in order to collect data for comparison to previously published results as well as to establish a standard by which flow through non-circular test orifices could be compared. An equilateral triangular cross-sectional area was chosen as the non-idealized orifice geometry both for the relative simplicity in manufacturing and the distinct non-circular pattern. Certainly, a triangular orifice is the most extreme non-circular cross-section as increasing the number of linear sides (four, five, six, . . .) of a constant area polygon approaches a more circular cross-sectional area in the limit. Also, for equivalent area cross-sections with fewer sides, the triangular shape results in the maximum perimeter for gas contact.

Orifices were manufactured with the use of standard 1/2" galvanized steel pipe caps and custom-made orifice inserts. Circular holes were accurately drilled into the cap centers and reamed with precision stainless steel bits; hand-sanding eliminated burrs from the flow passage entrance. The hole rims were lathed to thicknesses approximately 75% of the respective final orifice hole diameters. Triangular orifices were fabricated by first manually filing and polishing short sections of steel rod stock into approximately equilateral triangular cross-sectional geometries. These steel forms were coated with oil as a release agent and fixed in an upright position in a wooden block. Next, epoxy glue was spread around the forms and allowed to air-dry overnight. Once hardened, the epoxy disc was removed from the shaped rod and sanded with paper of number 600 grit to thicknesses about 75% of the hydraulic diameter, smoothing both the upstream and downstream faces. Finally, along with reinforcing steel washers, the orifice disks were epoxied to the perimeters of significantly larger holes drilled into the cap centers. All orifices were visually inspected and flow channels further smoothed under 22.5X magnification. Both circular and triangular orifices are represented in Figures 4 and 5.

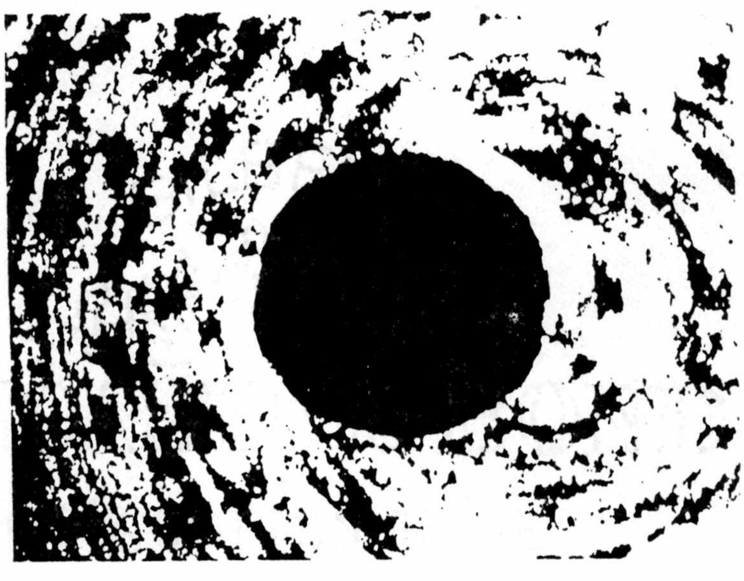

Figure 4. Photograph of Circular Orifice Number C1 Under 125X Magnification. (nominal diameter = 0.0421 inches)

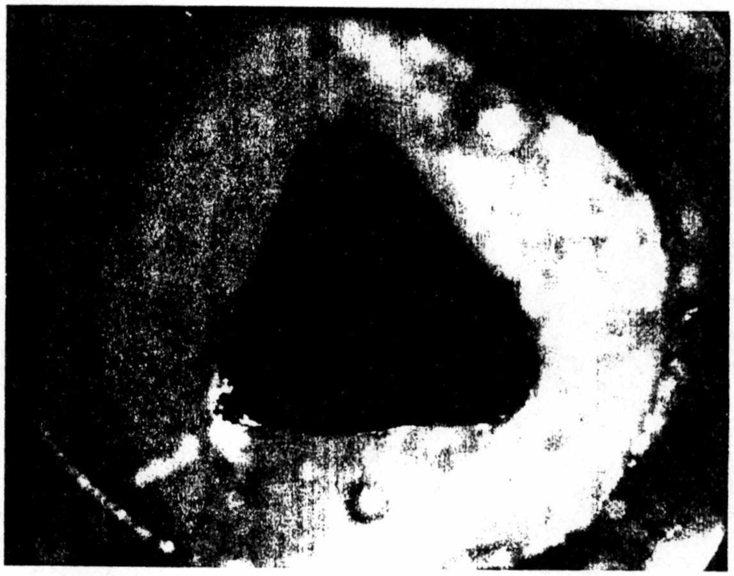

Figure 5. Photograph of Triangular Orifice Number T1 Under 125X Magnification. (nominal average side length = 0.0489 inches)

Precision measurements of downstream orifice dimensions were made with a video caliper, Olympus Model BH2, accurate to 0.001 mm, under a magnification of 500X. Each orifice was measured on two separate occasions; all dimensions were determined three times and averages are listed in Tables 1 and 2. The greatest variations in reproducibility, specifically 0.01532" to 0.01659" for circular orifice number C4, stem from eccentricity and diameter irregularities. Measurement variations are also due to problems with both focus and contrast as well as difficulty in determining the precise location of orifice boundaries under magnification. Both the upstream and downstream faces of the triangular orifices were measured before mounting in caps. Orifice thickness was determined with a digital micrometer and checked with a dial indicator.

The largest orifice diameter, 0.0421", and the 0.5" nominal internal pipe diameter yield a β ratio of about 0.084 and a velocity of approach factor, $\frac{1}{\sqrt{1 - \beta^4}}$, of about 1.0001. Thus, the assumption of negligible approach velocity is considered appropriate for this experimental arrangement.

Table 1. Circular Orifice Dimensions

Orifice Number	Average Diameter (in) ($\pm$ 0.0003")	Area (in^2)	Thickness (in), (% of hydraulic dia.)	Diameter Ratio β
C1	0.0421	1.39 E-3	0.0307 (73%)	0.08
C2	0.0294	0.68 E-3	0.0213 (72%)	0.06
C3	0.0208	0.34 E-3	0.0163 (78%)	0.04
C4	0.0162	0.21 E-3	0.0137 (84%)	0.03

Table 2. Triangular Orifice Dimensions

Orifice Number	Average Side Lengths (in) (± 0.0003")			Area (in^2)	Hydraulic Diameter (in)	Thickness (in), (% of hydraulic dia.)
	a	b	c			
T1	.0488	.0498	.0482	1.04 E-3	0.0282	0.0204 (72%)
T2	.0391	.0391	.0391	0.67 E-3	0.0227	0.0170 (75%)
T3	.0324	.0328	.0312	0.45 E-3	0.0185	0.0141 (76%)
T4	.0198	.0214	.0205	0.18 E-3	0.0119	0.0100 (84%)

SYSTEM COMPONENTS AND EXPERIMENTAL SET-UP

A photograph and a schematic representation of the experimental apparatus are shown in Figures 6 and 7. A twenty gallon storage capacity, two cylinder Sears Model MO-6436 electric compressor was used to supply air at 120 psig. A regulator/filter (Sears Model 282-160233) was used to reduce supply pressure to 100 $\pm$2 psig for leakage testing. This filter was used to remove particulate matter as well as liquid water from the air stream. To ensure constancy in supply pressure, a five gallon storage tank in a parallel piping arrangement was used to provide a system capacitance. Volumetric flow was measured with a United Cities' Model AL-800 aluminum-cased positive displacement reciprocating diaphragm meter rated for high pressure. Specifications indicated a pressure drop across the meter of less than 1/2" water column which was assumed negligible. Downstream from the diaphragm meter in parallel arrangement, three flow floatmeters with overlapping ranges were installed to check for the presence of flow pulsations. A parallel line fed directly to a precision test pressure gauge with an estimated measurement error less than 1% and finally to the test orifice. Feed-up piping was mostly 0.375" copper tubing with brass, compression fit unions. The steel orifice caps, however, were threaded onto 0.5" steel piping 5" in length. All external pipe threads were wrapped with Teflon tape before connection and routinely inspected for leakage and re-sealed as needed.

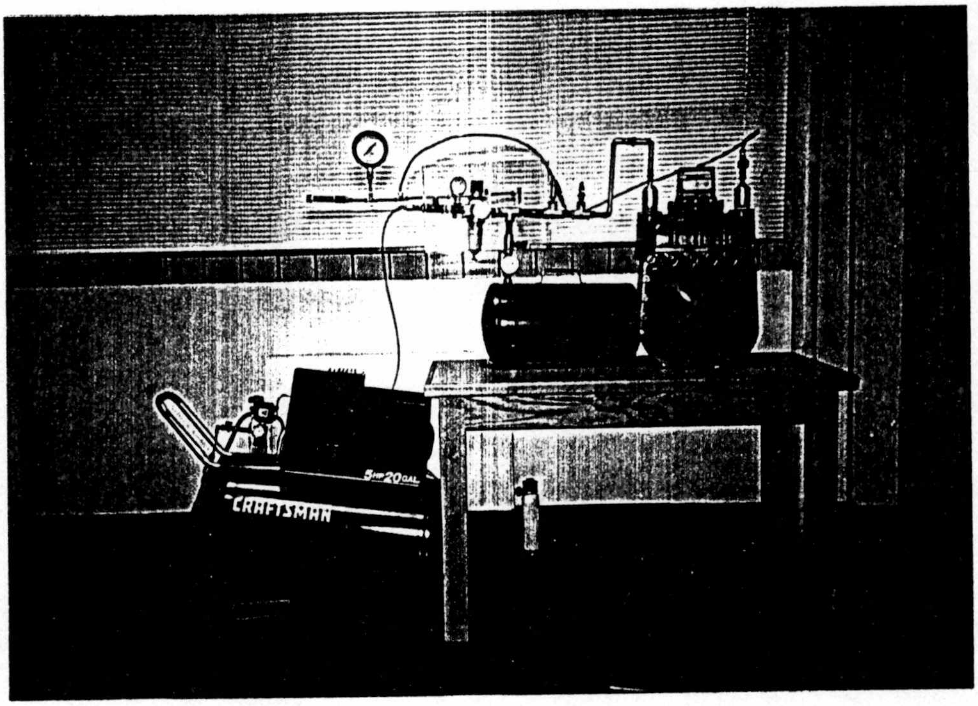

Figure 6. Photograph of Experimental Compressed Air Orifice Flow Metering System.

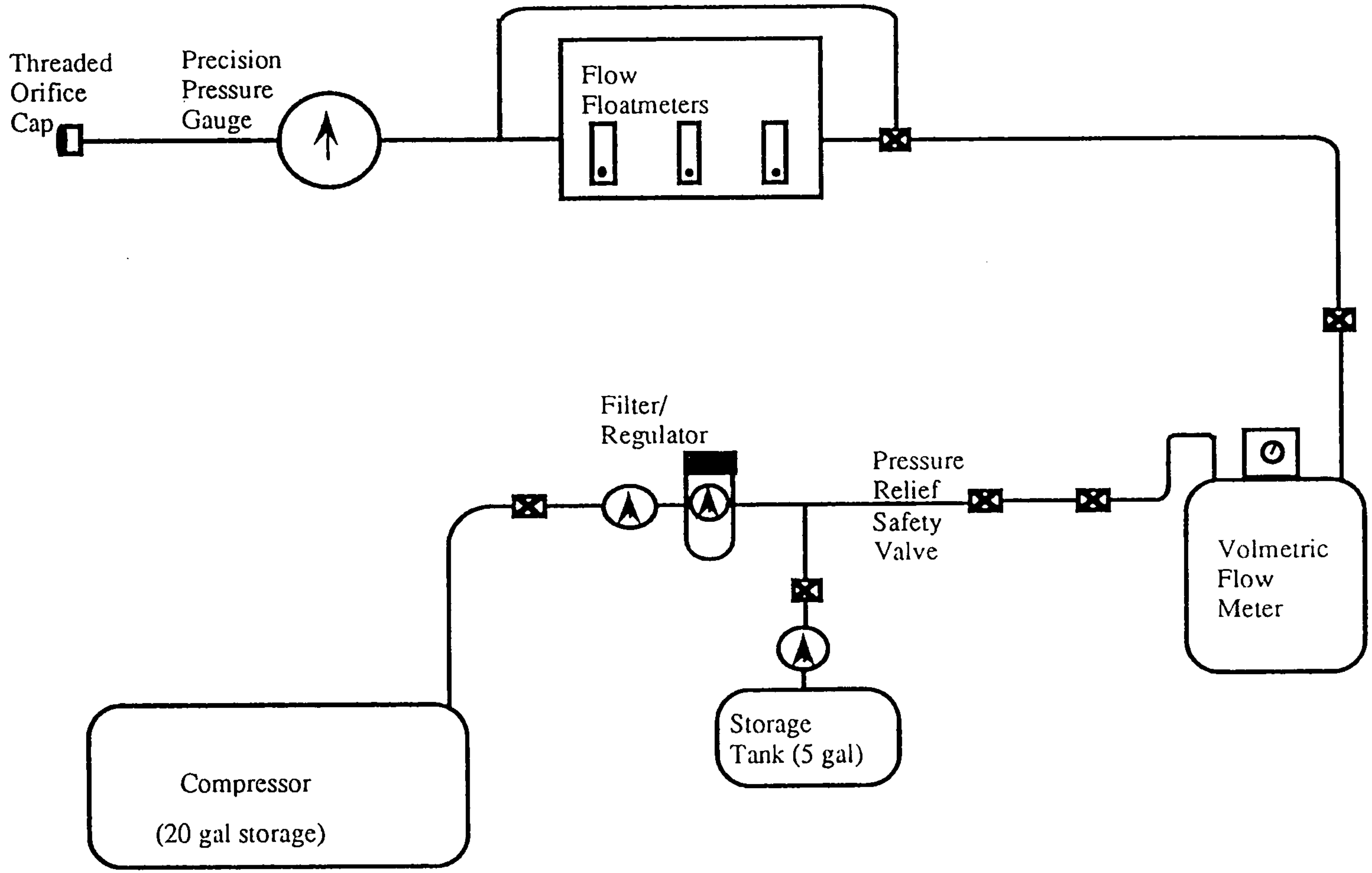

Figure 7. Schematic Representation of Experimental Compressed Air Orifice Flow Metering System.

EXPERIMENTAL PROCEDURES

In order to demonstrate the reproducibility of results obtained, repeated air flow measurements were indicated. Furthermore, as the timing of a metered volume of air discharged through each orifice was to be a manual procedure, in addition to the probable non-linear linkages within the meter itself, it was desired to obtain averaged quantities, again necessitating testing repetition. The effects of other variable parameters on the discharge rate were also considered. Specifically, the influence of slight pressure fluctuations on the flow rate was studied by sequentially increasing the supply pressure from ambient to 105 psig in approximate increments of 5 psig. Also, the effect of temperature changes was investigated by conducting two experimental runs on days when the laboratory ambient temperature differed by at least 10 ^{o}F.

Repeated air flow rate measurements were made for each of the orifice caps listed in Tables 1 and 2 by following the protocol described below. System leakage, which had a significant effect on measurement accuracy especially for the smallest orifices, was checked before every experimental run by sealing the inlet and outlet, pressurizing the system, and then inspecting all non-soldered unions with soapy water for the appearance of bubbles. If a leak was noted, fittings were resealed with Teflon tape, tightened, and rechecked.

A selected orifice was visually inspected for surface cleanliness under 22.5X magnification, screwed onto upstream piping, and the system was pressurized to 100 psig. A flow valve was opened and tests were conducted only after regulated pressure fluctuations (as observed on the precision pressure gauge) had been minimized. In most cases the achievable range was about ±2%; the higher value corresponded to the point in time when the compressor cycled on and the lower value to the preceding period. Relative equilibration occurred after about three compressor loading cycles. The small pressure variations which occurred were likely the result of limitations in the function of the pressure regulator used.

Volumetric air flow through the meter was indicated by a pointer on a 1" diameter analog dial divided into ten segments. Each of the ten marks corresponded to the discharge of 0.5 ft^3 of air at 100 psig; pointer movement around the entire dial represented the discharge of 5.0 ft^3 of air. Volumetric flow rate measurements of the discharge of 0.5 ft^3 of 100 psig air through the orifice to atmospheric pressure were made by timing the pointer movement from one marking to the next with a Fisher-Heurer analog stop watch the accuracy of which was checked against an electric digital clock over 60 second intervals indicating accuracy greater than 99.6%. The timing procedure utilized, however, was a manual process and thus, significantly variable.

For each experimental run, ten time measurements were made, with each run repeated at least four times; a total of no fewer than forty data points were gathered for all orifices except number T4. This cap ruptured during the second run; thus, only one experimental trial was completed. An experimental volumetric flow rate was calculated with the mean measured time recorded per discharge of 0.5 ft^3 of air; this value multiplied by air density at 100 psig calculated from the ideal gas law for each run yielded mass flow rate. An overall discharge coefficient, C_d, was then calculated from Equation (2-25).

CHAPTER 4

RESULTS

PRELIMINARY FINDINGS

Plots of elapsed time per nominal 0.5 ft^3 of flow as reflected in the gas flow meter 5 ft^3 dial pointer position, Figures 8 and 9, are representative of the raw data collected. (Raw data, tabulated and graphed, for all orifices are included in Appendix A) The overall cyclic appearance of this curve is attributed to non-linear, mechanical linkages in the meter which is designed to record long time interval (typically one month) cumulative natural gas usage. The general hysteresis curve-path was studied for four experimental runs; standard deviation of measured times in the same meter dial pointer position for all experimental runs was within less than ten percent of the average value for all orifice caps tested. This characteristic curve cycled with the cumulative discharge of 5.0 ft^3 of air.

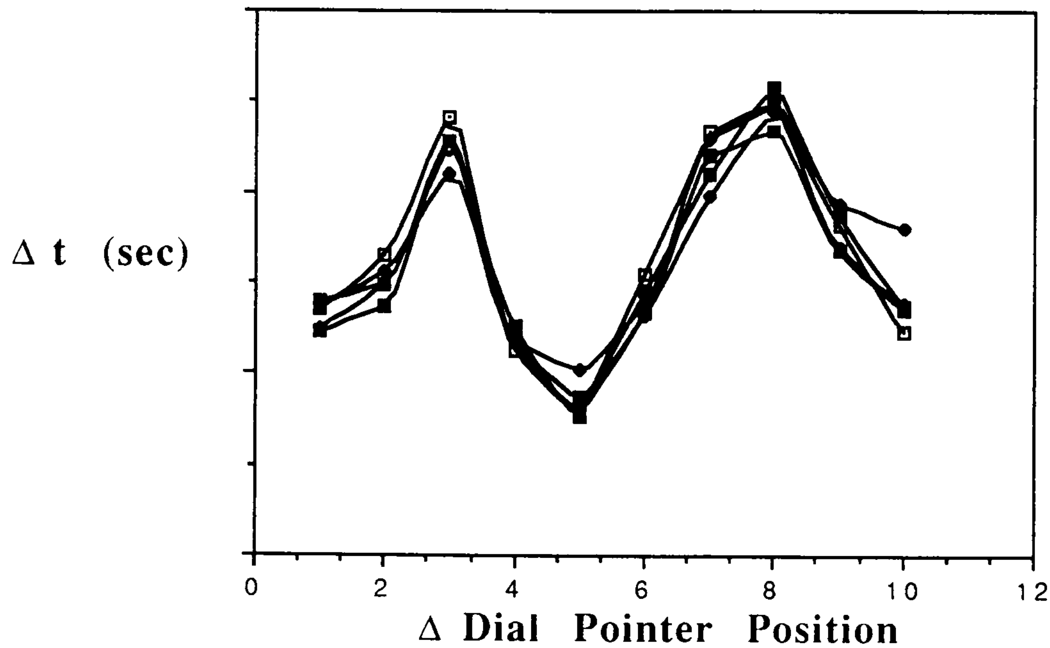

Figure 8. Measured Time Interval vs Change in Meter Dial Position for the Discharge of Air at 100 psig Through Circular Orifice C3, β=0.04.
Data for 4 runs included; dial position 10 represents one complete revolution of the dial pointer.

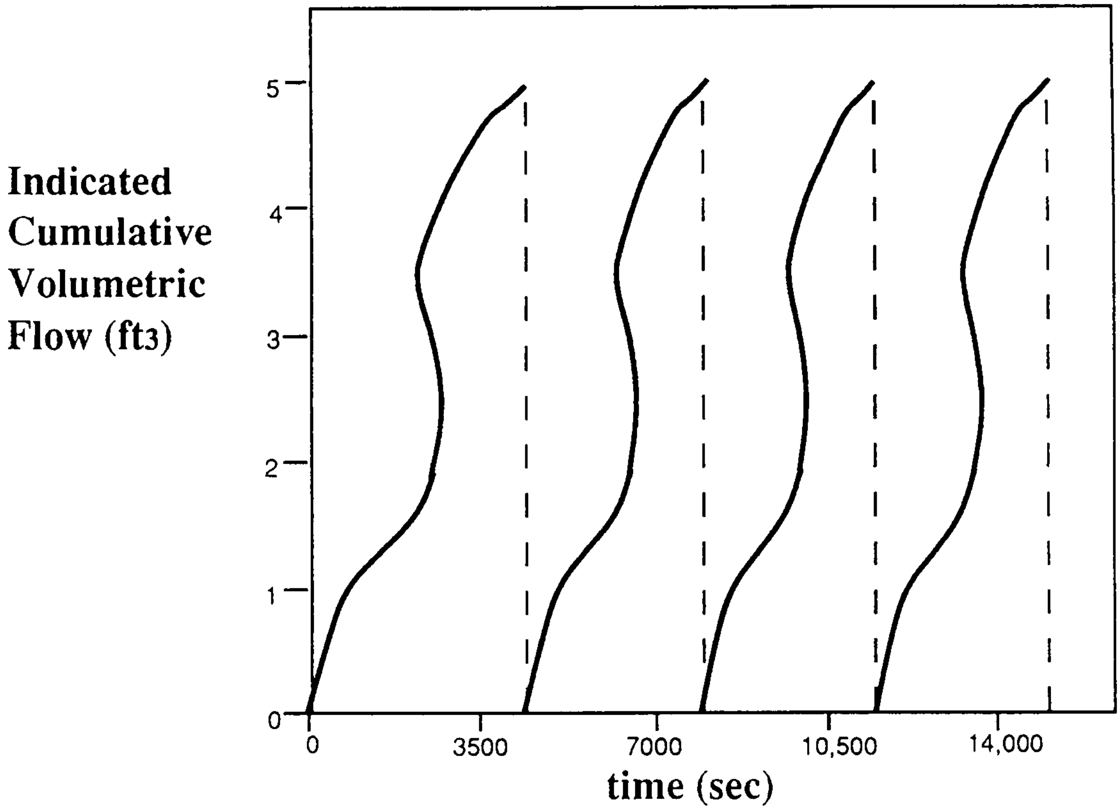

Figure 9. Illustrative Representation of Indicated Cumulative Volumetric Flow vs Time for the Discharge of Air at 100 psig Through Circular Orifice C3, β =0.04.

Time measurements over one cycle, specifically ten consecutive time measurements per flow of 0.5 ft^3, were arithmetically averaged; standard deviation of averaged times for different runs was less than 3% of average values for all orifices tested and may be attributed mainly to the manual variation inherent in the timing procedure. The ability to reproduce averaged volumetric flow rates to within 3% suggests that the data are highly repeatable and lends confidence to both the test flow apparatus and measurement procedure.

Laboratory ambient air temperature measured with both a precision mercury thermometer and a Cole-Parmer Model 8110-10 digital thermometer ranged from between 70°F to 80°F. Measured temperature of the air stream issuing from the orifice was approximately the same as room temperature. With manual control, system pressure fluctuations were not greater than 4 psig overall during any run.

DATA ANALYSIS

Experimentally measured volumetric flow discharge rates through orifices, calculated parameters, and test conditions are listed in Tables 3 and 4. Values presented correspond to the four experimental runs conducted for each of the circular and triangular orifices of various cross-sectional areas. Mean measured times represent an average of ten times recorded consecutively per discharge of 0.5 ft^3 of air. Air densities which ranged from 0.01795 $slug/ft^3$ to 0.01815 $slug/ft^3$ were calculated from the ideal gas law using measured ambient temperature. The overall discharge coefficient represents the ratio of mean measured flow rate to the calculated theoretical flow rate based on the isentropic choked flow of an ideal gas,

Table 3. Experimentally Measured Data and Calculated Parameters for Circular Orifices

Run Number	Relative Humidity of Air Entering (%)	Temperature of Air Entering (°F)	Supply Pressure (psig)	Air Density ($slug/ft^3$)	Mean Measured Time (sec) per 0.5 ft^3	Volumetric Flow Rate (ft^3/sec E-2)	Reynolds Number	Discharge Coefficient
		T_1	P_1	ρ	t	Q	Re	C_d
	$\beta = 0.08$							
C1 3/23	54	73	99<P<101	0.01805	90.1	0.5549	426,041	0.8683
C1 3/31	55	70	99<P<100	0.01815	91.9	0.5441	427,217	0.8623
C1 4/2a	53	70	99<P<101	0.01815	90.6	0.5519	427,217	0.8746
C1 4/2b	53	70	99<P<101	0.01815	92.3	0.5417	427,217	0.8585
	$\beta = 0.06$							
C2 3/23	54	73	100<P<102	0.01805	182.7	0.2737	297,520	0.8843
C2 3/31	55	70	100<P<102	0.01815	184.8	0.2706	298,341	0.8765
C2 4/6a	53	74	99<P<101	0.01801	185.2	0.2700	297,279	0.8713
C2 4/6b	53	74	99<P<101	0.01801	185.4	0.2697	297,279	0.8704
	$\beta = 0.04$							
C3 3/31	55	70	100<P<102	0.01815	370.4	0.1350	205,998	0.8752
C3 4/2	53	70	100<P<102	0.01815	365.3	0.1369	205,998	0.8875
C3 4/6a	53	74	99<P<101	0.01801	365.7	0.1367	205,264	0.8829
C3 4/6b	53	74	99<P<101	0.01801	357.6	0.1398	205,264	0.9029
	$\beta = 0.03$							
C4 3/31	55	70	100<P<102	0.01815	597.3	0.0840	168,451	0.8977
C4 4/2a	53	70	100<P<104	0.01815	589.6	0.0848	168,451	0.9063
C4 4/2b	53	70	100<P<104	0.01815	595.9	0.0840	168,451	0.8977
C4 4/2c	53	70	100<P<104	0.01815	594.7	0.0841	168,451	0.8988

Table 4. Experimentally Measured Data and Calculated Parameters for Triangular Orifices

Run Number	Relative Humidity of Air Entering (%)	Temperature of Air Entering (°F)	Supply Pressure (psig)	Air Density (slug/ft^3)	Mean Measured Time (sec) per 0.5 ft^3	Volumetric Flow Rate (ft^3/sec E-2)	Reynolds Number
		T_1	P_1	ρ	t	Q	Re
T1 3/23	54	73	98<P<102	0.01805	62.7	0.7974	285, 836
T1 3/26	60	72	98<P<102	0.01808	61.6	0.8117	286,085
T1 4/8a	64	76	97<P<101	0.01795	61.7	0.8104	285,038
T1 4/8b	64	76	97<P<101	0.01795	61.9	0.8078	285,038
T2 3/24	48	72	99<P<101	0.01808	125.3	0.3990	229,595
T2 4/7a	61	73	98<P<100	0.01805	125.4	0.3987	229,396
T2 4/7b	61	73	98<P<100	0.01805	124.0	0.4032	229,396
T2 4/8	64	72	98<P<100	0.01808	123.6	0.4045	229,595
T3 3/24	48	72	99<P<101	0.01808	169.7	0.2946	187,658
T3 4/7a	61	73	99<P<101	0.01805	169.8	0.2945	187,495
T3 4/7b	61	73	99<P<101	0.01805	170.1	0.2939	187,495
T3 4/7c	61	73	99<P<101	0.01805	170.4	0.2934	187,495
T4 3/24 ORIFICE RUPTURED	48	72	98<P<101	0.01808	375.1	0.1333	120,530

$$C_d = \frac{\dot{m}}{0.532 \frac{A P_o}{\sqrt{T_o}}} \qquad (4\text{-}1)$$

For the orifice flows encountered Reynolds numbers were calculated based on orifice hydraulic diameter as defined by the following equation:

$$Re_{D_h} = \rho V D_h/\mu \qquad (4\text{-}2)$$

Velocity of the air at the vena contracta was assumed to equal the maximum velocity reached thorough adiabatic expansion:

$$V_{max} = (2 c_p T_o)^{1/2} \qquad \text{Equation (2-13)}$$

where $c_p = 6010\ ft^2/(s^2\ {}^oR)$. Temperature gradients were considered small; "stagnation" temperature was taken as ambient and air viscosity was taken as a constant, $\mu = 3.8\ (10)^{-7}$ slug/(ft·s) at standard temperature and pressure. With these assumptions, the range of Reynolds numbers obtained for all orifices was not less than about 168,000 (for the smallest circular orifice) and not more than about 427,000 (for the largest circular orifice). As it is well documented (7) that the effect of Reynolds number on the discharge coefficient becomes approximately constant above Re = 100,000, the influence of this parameter has not been considered further in this work.

For comparison of the data obtained with the straight-edged circular orifices to previously documented results, the calculated discharge coefficients were plotted as functions of the dimensionless ratios of system to ambient air pressure and pipe to orifice diameter, β. Plots comparing triangular and circular orifice mean volumetric flow rates were constructed as functions of orifice cross-sectional area, hydraulic diameter, and perimeter.

GENERAL DISCUSSION OF FINDINGS

Two separate experimental runs with circular orifice cap number C2 were conducted at times when ambient temperature differed by 10 ^oF; room temperature was 70 ^oF during one trial and 80 ^oF during the second. Average times recorded per discharge of 0.5 ft^3 of air for both runs differed by only about 1%, which can be attributed to timing errors alone. Thus, the small ambient air temperature variations, 70 ^oF to 76 ^oF, between other trials were deemed important only for the calculation of air densities used in the determination of C_d and Re_d as defined in Equations (4-1,2).

Supply pressure (P) fluctuations were as small as $99 < P < 100$ psig to as large as $100 < P < 104$ psig during the various experimental runs. Therefore, the effects of this variation on the derived quantitative results was investigated. By sequentially increasing the supply pressure in approximate increments of 5 psig, discharge coefficients were calculated for a range of ratios of system to ambient pressures. Figure 10 illustrates the general type of curve obtained for discharge of air through an orifice for a critical flow regime. As Perry noted (6), the mass flow rate of compressed air through an orifice continue to rise with increased system pressure even in the choked-flow range. The flow continued to increase towards an ultimate maximum below a pressure ratio of about 0.15 for this investigation. The ratio of experimental ambient (14.7 psia) to system pressure (114.7 psia), 0.13, fell below this point and thus, the minor variations in pressure, about ±2%, were considered to have minimal effect on the measured flow rates.

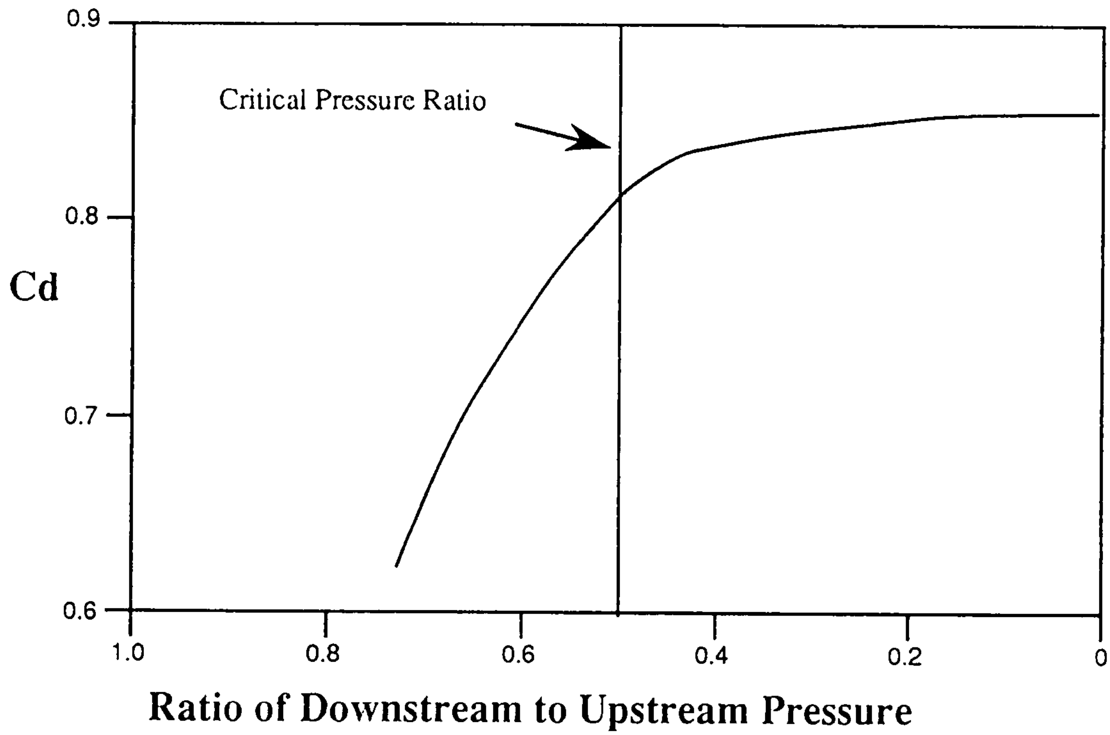

Figure 10. Illustration of Discharge Coefficient vs Pressure Ratio for the Discharge of Air at 100 psig Through Circular Orifice C2, β =0.06.

Overall discharge coefficients obtained for the circular orifices are shown as a function of β in Figure 11. Standard deviation between mean measured discharge times was less than 3% for all orifices. Slight differences may be attributed primarily to variation in timing intervals and to uninvestigated roughness characteristics of the orifice throat. For a beta ratio of 0.08 the calculated discharge coefficient was determined to be about 0.87 and rose to more than 0.90 with correspondence to a diameter ratio of about 0.03. Reliability of the calculated discharge coefficient depended significantly upon the quality of the corresponding orifice area measurement, especially for smaller areas, due to the inversely proportional functional dependence of the discharge coefficient on orifice area (Equation 4-1). As orifice cross-sectional area decreased, microscopic measurement of overall dimensions was more difficult and relative error increased.

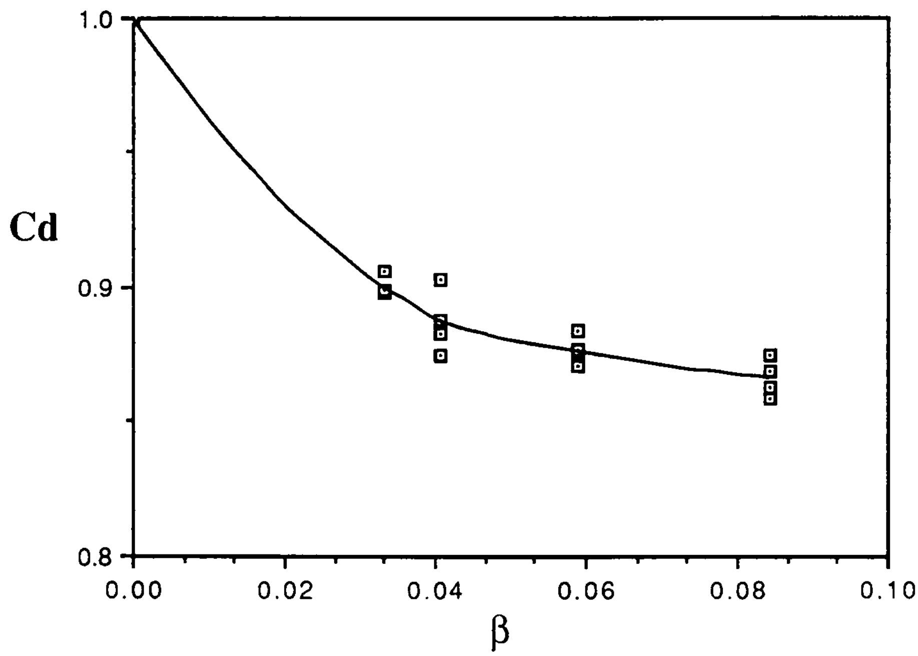

Figure 11. Discharge Coefficient vs Beta Ratio for the Discharge of Air at 100 psig Through Straight-Edged Circular Orifices C1, C2, C3, and C4 for 4 Repeated Measurements.

In Figure 12 the discharge coefficients obtained with straight-edged circular orifices used in this investigation are compared to re-plotted data gathered by Grace and Lapple (18) for knife-edged circular orifice plates and sonic flow nozzles of similar beta ratios. Discharge coefficients predicted in this experiment are less than those obtained with critical flow nozzles, as expected, but are notably about 5% higher than those indicated by Grace for the knife-edged orifices. This apparent discrepancy is most probably explained by variations in the thicknesses of the respective orifices and the influence of this parameter on the efflux. Thicknesses of the straight-edged circular orifices ranged from about 0.02 to 0.03 inches, whereas, the thicknesses of Grace's knife-edged orifice plates were not more than 0.002 inches in all cases. Grace's work demonstrated that, for large Reynolds numbers, increased orifice throat thickness resulted in a decreased degree of vena contracta and, as a result, an increased mass flow rate. For this reason the obtaining of a higher range of discharge coefficient is expected.

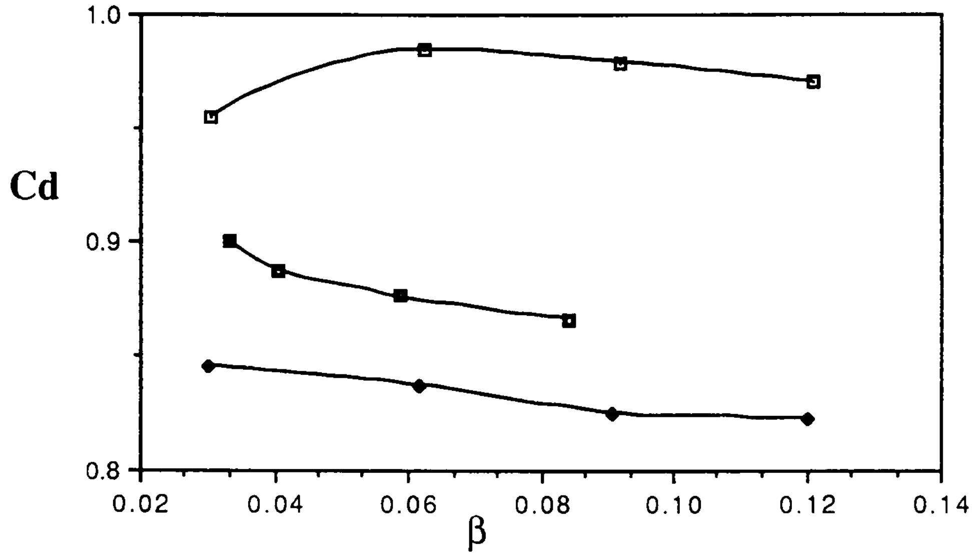

Figure 12. Discharge Coefficient vs Beta Ratio for Knife- and Straight-Edged Circular Orifices and Nozzles for the Discharge of Air at 100 psig.

- ◻ Data from Grace for the discharge of air at 100 psig through a nozzle.
- ■ Present investigation, experiment was conducted for the discharge of air at 100 psig through circular orifices, numbers C1, C2, C3, and C4 for 4 repeated measurements.
- ◆ Data from Grace for the discharge of air at 100 psig through circular orifices.

(Adapted from: H.P. Grace and C.E. Lapple, Discharge Coefficients of Small-Diameter Orifices and Flow Nozzles, Trans. ASME, Vol.73, 1951, p.645.)

Measured volumetric discharge rates obtained with both triangular and circular orifices plotted against actual orifice areas are shown in Figure 13. As a general result flow rates through the triangular orifices were about 30% higher than those through a circular for orifices of similar cross-sectional areas. A comparable plot (Figure 14) was obtained by graphing flow rate versus orifice hydraulic diameter. Defined as four times the wetted perimeter divided by cross-sectional area (4p/A), the hydraulic diameter is a typical means by which frictional processes of flows through pipes of different cross-sectional geometries are compared. However, even as the basis of a hydraulic diameter "normalization," discharge through the triangular orifice was again substantially greater than that through the circular orifice. In striking contrast to this result is Figure 15, a graph of volumetric flow rate versus orifice perimeter. Notably, the plots coincide for both the triangular and circular orifice geometries, indicating similar volumetric flow rates through equilateral triangular and circular orifices of equal cross-sectional perimeter. This occurrence may be due in part to the observed reduction in degree of vena contracta for flow discharge through a triangular orifice as compared to that through a circular orifice of similar cross-sectional area.

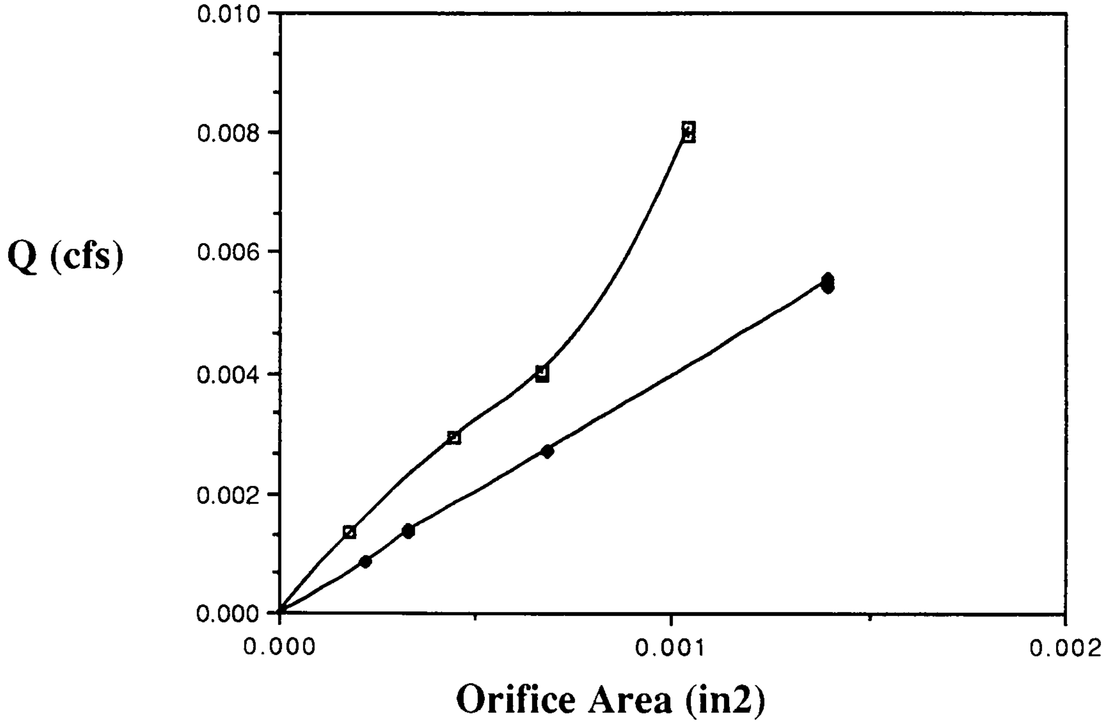

Figure 13. Volumetric Flow Rate vs Orifice Area for the Discharge of Air at 100 psig.

- ▫ Volumetric flow rate through triangular orifices T1, T2, T3, and T4 for 4 repeated measurements (only 1 measurement made with T4).
- ♦ Volumetric flow rate through circular orifices C1, C2, C3, and C4 for 4 repeated measurements.

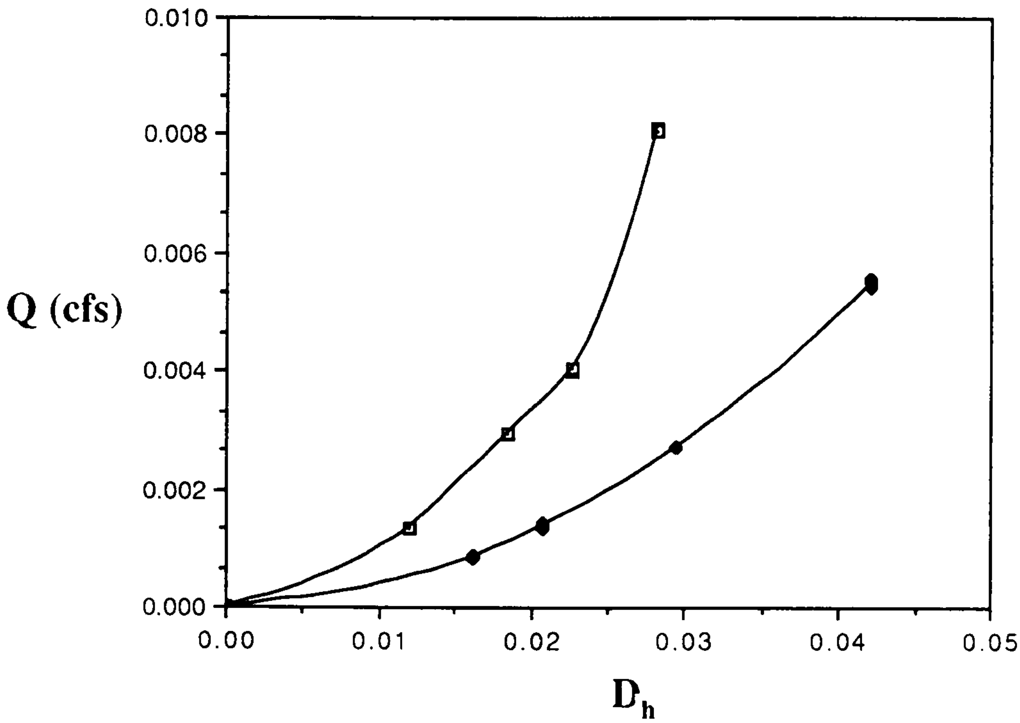

Figure 14. Volumetric Flow Rate vs Hydraulic Diameter for the Discharge of Air at 100 psig.

- ▫ Volumetric flow rate through triangular orifices T1, T2, T3, and T4 for 4 repeated measurements (only 1 measurement made with T4).
- ◆ Volumetric flow rate through circular orifices C1, C2, C3, and C4 for 4 repeated measurements.

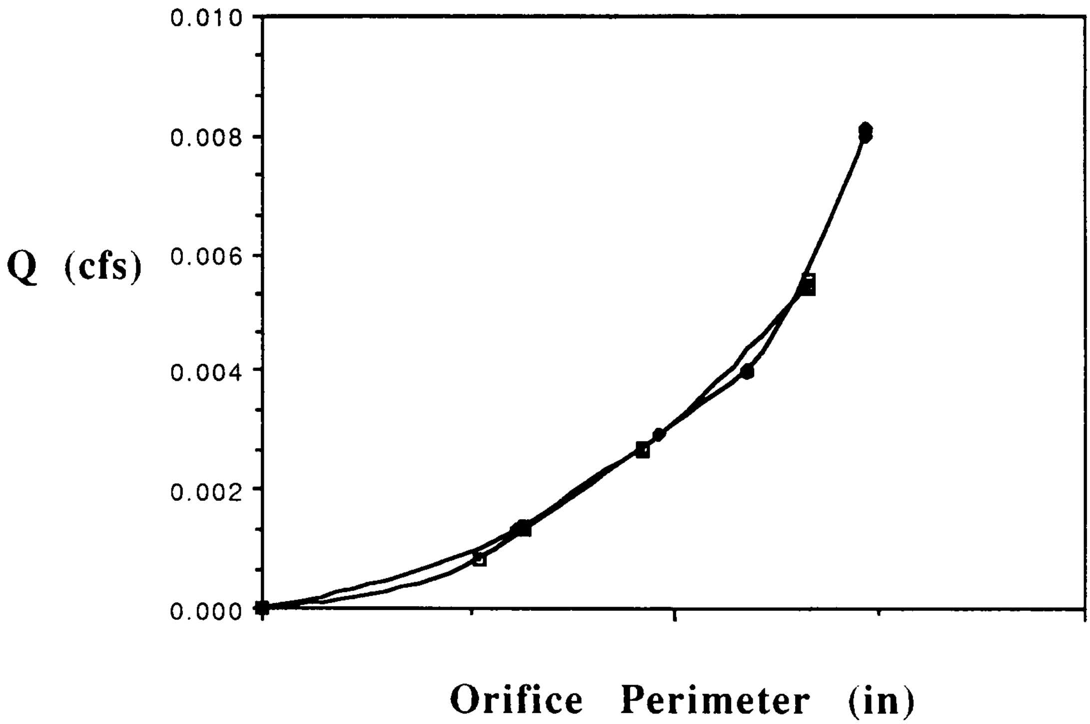

Figure 15. Volumetric Flow Rate vs Orifice Perimeter for the Discharge of Air at 100 psig.

- ◆ Volumetric flow rate through triangular orifices T1, T2, T3, and T4 for 4 repeated measurements (only 1 measurement made with T4).

- ▫ Volumetric flow rate through circular orifices C1, C2, C3, and C4 for 4 repeated measurements.

Figure 16 and Table 5 represent calculated discharge coefficients with respect to inscribed (defined by hydraulic diameter) and circumscribed circular and triangular areas. Based upon both inscribed circular area and actual triangular area, C_d was calculated to be greater than unity; predicted in terms of circumscribed circular area, C_d was less than 1.0. As the discharge coefficient represents a fraction of ideal flow, it appears that the discharge coefficient for triangular orifices appears best defined in terms of a circumscribed area.

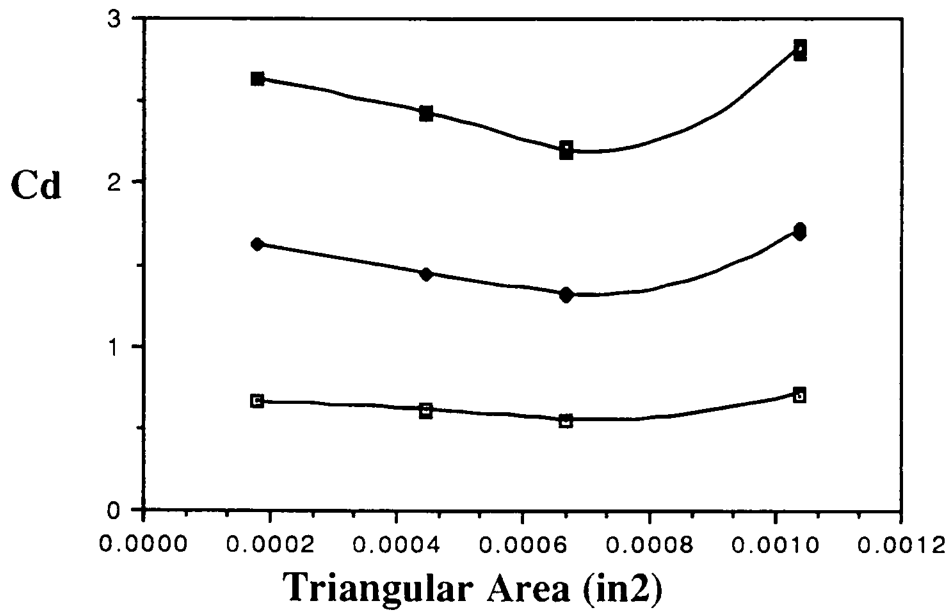

Figure 16. Discharge Coefficients for Triangular Orifices T1, T2, T3, and T4 Calculated for 4 Repeated Measurements with respect to Inscribed and Circumscribed Circular and Triangular Areas for the Discharge of Air at 100 psig.

- ■ Cd calculated with respect to inscribed circular area.
- ◆ Cd calculated with respect to triangular area.
- □ Cd calculated with respect to circumscribed circular area.

Note, only 1 measurement made with orifice T4.

Table 5. Discharge Coefficients Calculated for Air Flow Through Triangular Orifices

Run Number	Volumetric Flow Rate (ft^3/sec E-2)	Discharge Coefficient relative to Inscribed Circular Area	Dishcharge Coefficient relative to Triangular Area	Dishcharge Coefficient relative to Circumscribed Circular Area
	Q	C_{di}	C_{dt}	C_{dc}
T1 3/23	0.7974	2.7869	1.6894	0.6969
T1 3/26	0.8117	2.8391	1.7209	0.7099
T1 4/8a	0.8104	2.8247	1.7127	0.7063
T1 4/8b	0.8078	2.8156	1.7067	0.7040
T2 3/24	0.3990	2.1917	1.3142	0.5480
T2 4/7a	0.3987	2.1885	1.3121	0.5472
T2 4/7b	0.4032	2.2132	1.3269	0.5534
T2 4/8	0.4045	2.2219	1.3323	0.5556
T3 3/24	0.2946	2.4307	1.4505	0.6078
T3 4/7a	0.2945	.204287	1.449	0.6071
T3 4/7b	0.2939	2.4237	1.4460	0.6059
T3 4/7c	0.2934	2.4195	1.4436	0.6049
T4 3/24	0.1340	2.6283	1.6222	0.6571

CHAPTER 5

CONCLUSIONS AND RECOMMENDATIONS FOR FURTHER STUDY

The experimental results discussed in this paper have shown that the volumetric flow rate of compressed air at 100 psig issuing from an essentially stagnant reservoir through a thin, triangular-shaped orifice to atmospheric conditions is about 30% greater than through a circular orifice of equal cross-sectional area. It is noted that for steady, fully-developed duct flows a circular passage is certainly the hydrodynamically optimal configuration; flow rate through an equilateral triangular duct would only be about 70% of that through a circular duct (19). Orifice flow of a compressible gas, however, does not approximate such a well-modeled, fully-developed flow situation. It more closely resembles turbulent jet flow, characterized by a creeping flow marked with nested eddies which is suddenly accelerated through a minimal throat length. Thus, it is not surprising that while the hydraulic diameter idea closely approximates turbulent flows for a variety of duct shapes, it is not appropriate to apply this concept to flow through a thin orifice.

Graphical data presented indicate similar discharge flow rates for both triangular and circular orifices equal in perimeter. Between orifices equal in area, the triangular perimeter is of course larger than the corresponding circular one, and in this case flow was about 30% greater through the triangle. (It is interesting to note that for incompressible turbulent jet flow (20), mean flow velocity decays more rapidly for a circular jet than for a plane jet.) While the larger perimeter ratio of triangle to circle may in part explain an increased mass flow rate, its impact on the additional issues of acceleration, compressibility, and three-dimensional effects, all of which partly determine downstream flow pattern, is of importance. It was observed that the rate of efflux expansion was more through a triangular orifice than through a circular one of equal area. This degree of vena contracta governs the rate of mass flow through an orifice and is largely determined by the upstream orifice dimensions. Therefore, it is concluded that in relating flows through thin triangular and circular orifices, the orifice perimeter is of primary significance.

For future studies an improvement of flow metering techniques would be warranted. For example, the flow meter analog dial could be replaced with an electric transducer and microprocessor for improved volumetric flow metering. Manual timing procedures could be replaced with an automatic system which would record time intervals electrically in the microprocessor system.

An attractive area for further work would be an extended study of compressed air flows through differing non-circular orifice geometries. It is hypothesized that as the number of linear sides is increased for a constant cross-sectional area, the mass flow rate would begin to approach that of discharge through a circular orifice.

Also, attention should be given to orifices of other than equilateral linear geometries, such as a rectangle, and to those with non-linear boundaries, for example an oval since actual industrial leaks likely occur through a wide variety of flow geometries. The effect of orifice length to width or eccentricity ratios on the discharge rate and efflux pattern should be investigated.

Another extension of this work would be the study of leakage sound characteristics for a variety of orifice geometries in order to identify frequency patterns possibly unique to particular leak geometries and their associated discharge flow rates. Such relationships may be useful in the development of methods of measurement of single leak air flow loss rates for actual industrial leaks.

Finally, for few leakage sites of small cross-sectional area, mass flow rate prediction tables based on one-dimensional, critical, compressible flow theory for the discharge of air through an idealized circular orifice provide an adequate, order-of-magnitude estimate of air lost. However, for the numerous leakage sites typically found in an industrial setting such tables significantly underestimate the total amount of leaking compressed air and the amounts of lost energy and money. Therefore, based upon the demonstrated importance of orifice perimeter, it is recommended that when estimating leakage air loss with flow rate tables, data comparisons for similar perimeters, leak to circular orifice, be made rather than for estimated circular leak areas.

LIST OF REFERENCES

1. United States Department of Energy, "Compressed Air Systems: A Guidebook on Energy and Cost Savings," National Technical Information Service, Springfield, VA, 1984, p.1.

2. U.S. DOE, "Compressed Air Systems," p.141.

3. R. Jendrucko and K. Binkley, Factors Affecting the Implementation of Energy Conservation Measures Identified During Audits of Manufacturing Facilities, Power Generation, Energy Management and Environmental Sourcebook, *Proc. of the 14th World Energy Engineering Congress*, 1991, p. 433.

4. F.M. White, "Fluid Mechanics," McGraw-Hill, New York, N.Y., 1986, p.513.

5. A.H. Shapiro, "Dynamics and Thermodynamics of Compressible Fluid Flow," vol. 1., The Ronald Press Co., New York, N.Y., 1953, pp.73-75, 85, 100.

6. J.A. Perry, Jr., Critical Flow Through Sharp-Edged Orifices, *Trans. ASME*, vol. 71, 1949, pp.757-764.

7. Ingersoll-Rand, Compressors Accessories Catalog A, Distributor Publications, Stamford, CT, 1978, p.163.

8. R.H. Perry, "Perry's Chemical Engineer's Handbook," 6th ed., McGraw-Hill, New York, N.Y., 1984, pp. (5-11)-(5-13).

9. T. Baumeister, "Marks' Standard Handbook for Mechanical Engineers," 8th ed., McGraw-Hill, New York, N.Y., 1978, pp. (4-46)-(4-48).

10. H.B. Reynolds, The Flow of Air and Steam Through Orifices, *Trans. ASME*, vol.38, 196, p. 799.

11. H. Bean, E. Buckingham, and P. Murphy, Discharge Coefficients of Orifices, National Bureau of Standards, *J. of Research*, vol. 2, 1929, pp.561-658.

12. Orifice Metering of Natural Gas, American Gas Association, Report 3, Arlington, Va., 1985.

13. K. Hall, Derivation of Orifice Equations Reevaluated, *Oil and Gas Journal*, July 1983, pp. 66-69.

14. R.J. Goldstein, "Fluid Mechanices Measurements," Hemishphere Publishing Corp., New York, N.Y., 1983, p.298.

15. Shapiro, 358-360.

16. T. Fox and J. Stark, Characteristics of Miniature Short-Tube Orifice Flow, *Proc. of the Institute of Mechanical Engineers*, vol. 203, no. 5, 1989, pp. 351-358.

17. H. Linden and D. Othmer, Air Flow Through Small Orifices in the Viscous Region, *Trans. ASME*, vol. 71, 1949, pp. 765-772.

18. H. Grace and C. Lapple, Discharge Coefficients of Small Diameter Orifices and Flow Nozzles, *Trans. ASME*, vol. 73, 1951, pp. 639-647.

19. F.M. White, "Viscous Fluid Flow," McGraw-Hill, New York, N.Y., 1974, p.121.

20. F.M. White, "Viscous Fluid Flow," p. 512.

APPENDIX

Table 6. Raw Data Collected with Circular Orifice C1

	Run Number			
Measured	**C1 3/23**	**C1 3/31**	**C1 4/2a**	**C1 4/2b**
Time(sec)	89	94	87	90
per	97	103	94	101
0.5 ft^3	109	96	100	103
of Air	86	87	84	90
Flow	69	69	73	68
	76	86	90	84
	95	97	93	102
	100	108	109	110
	99	100	95	96
	81	79	81	79

Table 7. Raw Data Collected with Circular Orifice C2

	Run Number			
Measured	C2 3/23	C2 3/31	C2 4/2a	C2 4/2b
Time(sec)	190	190	194	193
per	193	198	200	200
0.5 ft^3	181	182	186	185
of Air	151	180	172	180
Flow	134	147	145	147
	159	167	160	162
	221	217	213	208
	220	215	219	224
	186	195	206	200
	162	157	157	155

Table 8. Raw Data Collected with Circular Orifice C3

	Run Number			
Measured	**C3 3/31**	**C3 4/2**	**C3 4/6a**	**C3 4/6b**
Time(sec)	338	339	339	322
per	368	359	349	346
0.5 ft^3	444	413	428	420
of Air	316	322	326	314
Flow	281	275	277	277
	357	342	345	329
	437	433	410	425
	452	451	458	441
	385	397	388	367
	326	322	337	335

Table 9. Raw Data Collected with Circular Orifice C4

	Run Number			
Measured	C4 3/31	C4 4/2a	C4 4/2b	C4 4/2c
Time(sec)	612	592	612	616
per	636	630	622	640
0.5 ft^3	675	671	666	667
of Air	554	553	557	557
Flow	427	430	450	446
	554	531	546	540
	635	634	630	623
	715	714	725	720
	626	629	637	630
	539	512	514	508

Table 10. Raw Data Collected with Triangular Orifice T1

	Run Number			
Measured	**T1 3/23**	**T1 3/26**	**T1 4/8a**	**T1 4/8b**
Time(sec)	63	66	60	61
per	72	73	71	69
0.5 ft^3	62	60	65	64
of Air	57	58	60	58
Flow	50	48	49	47
	70	69	67	64
	75	76	72	74
	64	60	71	77
	58	57	53	54
	56	49	49	51

Table 11. Raw Data Collected with Triangular Orifice T2

	Run Number			
Measured Time(sec) per 0.5 ft^3 of Air Flow	**T2 3/24**	**T2 4/7a**	**T2 4/7b**	**T2 4/8**
	121	122	122	126
	135	132	130	130
	142	146	132	136
	115	116	118	114
	101	91	94	102
	122	128	115	111
	134	131	138	144
	149	146	153	146
	127	133	130	126
	107	109	108	101

Table 12. Raw Data Collected with Circular Orifice T3

	Run Number			
Measured	T3 3/24	T3 4/7a	T3 4/7b	T3 4/7c
Time(sec)	170	176	172	171
per	194	182	199	200
0.5 ft^3	198	200	182	194
of Air	159	160	160	154
Flow	97	98	98	96
	166	165	177	159
	185	187	189	193
	200	206	195	197
	180	174	182	177
	148	150	147	163

Table 13. Raw Data Collected with Circular Orifice T4

Run Number	
Measured	T4 3/24
Time(sec)	390
per	395
0.5 ft^3	401
of Air	330
Flow	363
	385
	397
	380
	362
	348

Table 14. Raw Data Collected with Circular Orifice C2 Throughout a Range of Pressure Ratios.

Supply Pressure (psig)	**Mean Measured Time (sec)/ 0.5 ft^3**
5	2586
20	1942
40	1920
60	1892
80	1888
90	1873
95	1872
100	1876
105	1878

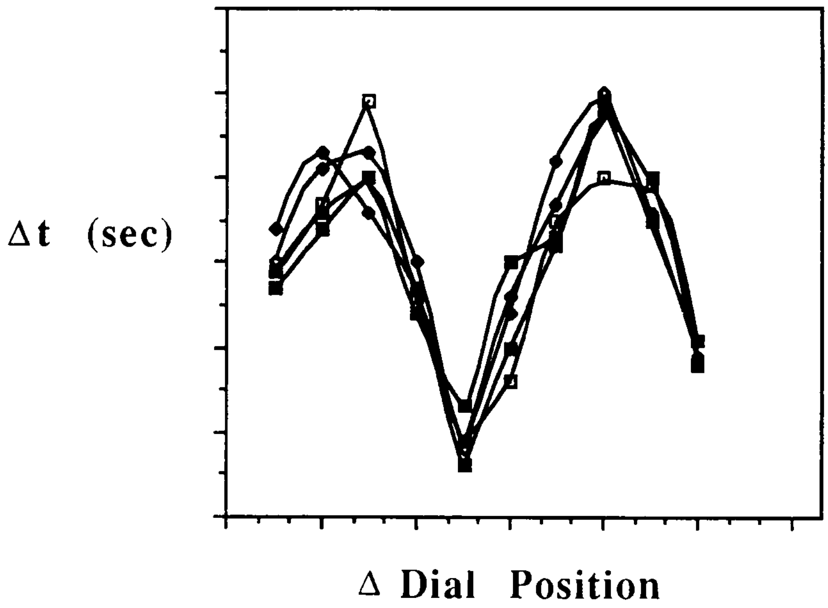

Figure 17. Measured Time Interval vs Change in Meter Dial Pointer Position for the Discharge of Air at 100 psig Through Circular Orifice C1, β=0.08.
Data for 5 runs included; dial position 10 represents one complete revolution of the dial pointer.

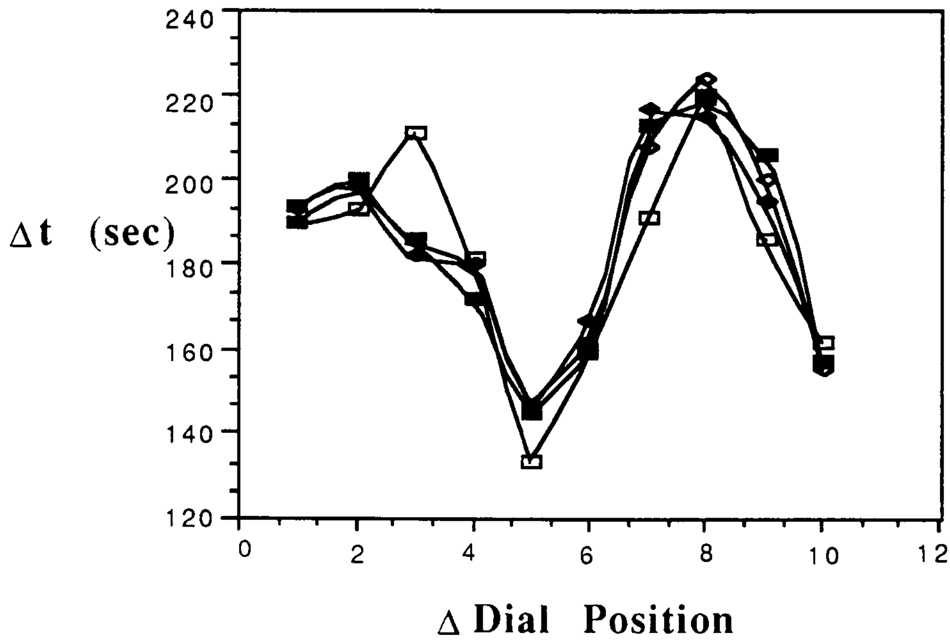

Figure 18. Measured Time Interval vs Change in Meter Dial Pointer Position for the Discharge of Air at 100 psig Through Circular Orifice C2, β=0.06.

Data for 4 runs included; dial position 10 represents one complete revolution of the dial pointer.

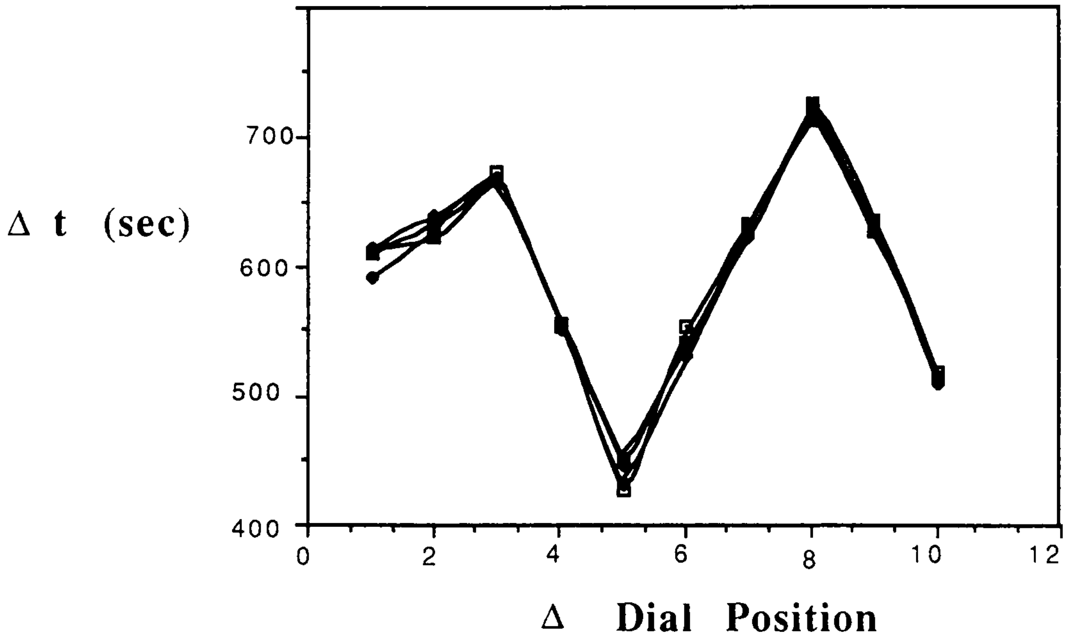

Figure 19. Measured Time Interval vs Change in Meter Dial Pointer Position for the Discharge of Air at 100 psig Through Circular Orifice C4, β=0.03.

Data for 4 runs included; dial position 10 represents one complete revolution of the dial pointer.

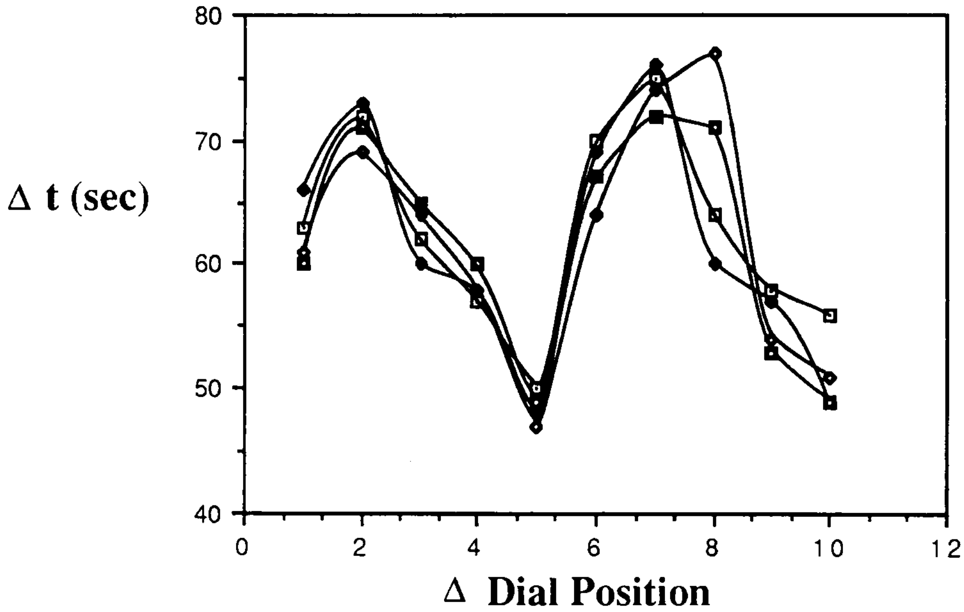

Figure 20. Measured Time Interval vs Change in Meter Dial Pointer Position for the Discharge of Air at 100 psig Through Triangular Orifice T1.
Data for 4 runs included; dial position represents one complete revolution of the dial pointer.

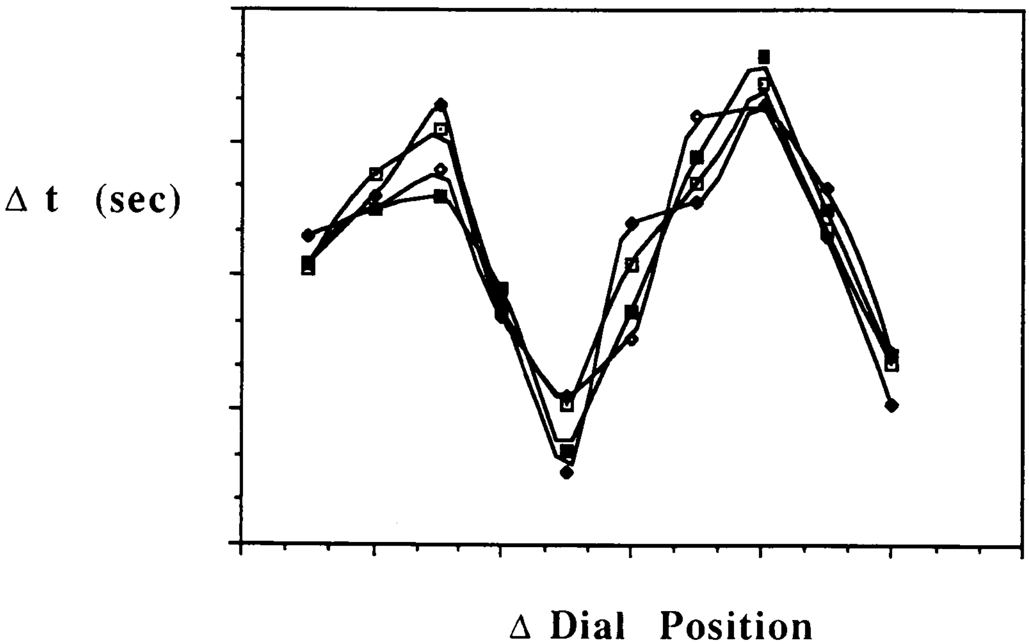

Figure 21. Measured Time Interval vs Change in Meter Dial Position for the Discharge of Air at 100 psig Through Triangular Orifice T2.

Data for 4 runs included; dial position 10 represents one revolution of the dial pointer.

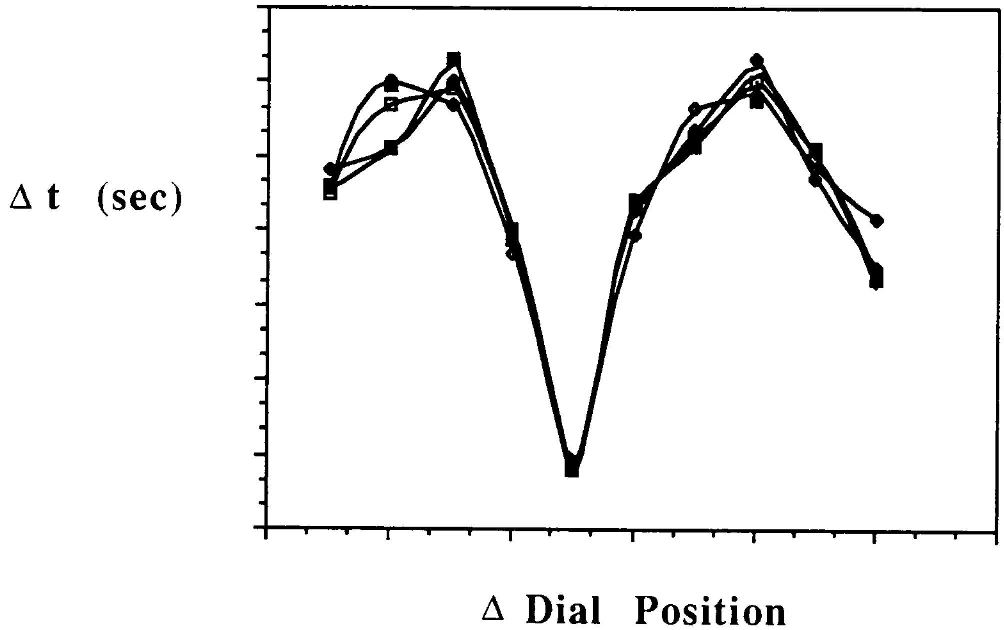

Figure 22. Measured Time Interval vs Change in Meter Dial Pointer Position for the Discharge of Air at 100 psig Through Triangular Orifice T3.
Data for 4 runs included; dial position 10 represents one complete revolution of the dial pointer.

VITA

Rebecca Ann Bachschmidt was born in Knoxville, Tennessee on October 28, 1967. She attended elementary schools in the Knox County School District and graduated from Halls High School in 1985. The following September she entered the University of Tennessee, Knoxville and in May 1990 received the degree of Bachelor of Science in Engineering Science. She began graduate studies at the University of Tennessee, Knoxville the following fall semester and in August, 1992 received a Master of Science degree in Engineering Science.